HYDROLOGY OF THE FOREST CITY BASIN, MID-CONTINENT, USA: IMPLICATIONS FOR CO_2 SEQUESTRATION IN THE ST. PETER SANDSTONE

A Thesis

presented to

the Faculty of the Graduate School

at the University of Missouri-Columbia

In Partial Fulfillment

of the Requirements for the Degree

Master of Science

---

by

CHRISTOPHER R. BURROWS

Dr. Martin Appold, Thesis Supervisor

DECEMBER 2012

The undersigned, appointed by the dean of the Graduate School,

have examined the thesis entitled

HYDROLOGY OF THE FOREST CITY BASIN, MID-CONTINENT, USA:

IMPLICATIONS FOR CO_2 SEQUESTRATION IN THE ST. PETER SANDSTONE

Presented by Christopher R. Burrows,

A candidate for the degree of

Master of Science

And hereby certify that, in their opinion, it is worthy of acceptance.

_____

Dr. Martin S. Appold

_____

Dr. Peter I. Nabelek

_____

Dr. John J. Bowders, P.E.

ACKNOWLEDGEMENTS

I would like to thank my advisor, Dr. Martin Appold, for all his help and guidance with this project and for his encouragement throughout my graduate and undergraduate careers. I would also like to thank my committee members, Dr. John Bowders and Dr. Peter Nabelek, for their input, as well as the Department of Geological Sciences at the University of Missouri for its financial support of my research. I would also like to acknowledge Mr. David Laflen of the Kansas Geological Survey, Dr. Ray Anderson of the Iowa Geological Survey, and the rest of the staffs at these facilities for their invaluable assistance in providing core samples for use in this study. In addition, I want to express my sincere appreciation for Dr. Julie Sheets of the Ohio State University and the staff of the SEMCAL facility for providing considerable insight and technical expertise which made possible the mineralogical analysis of the St. Peter Sandstone in this study. I must also thank Rachel Duckworth for all her help in the conductivity and porosity testing as well as field sampling and measurements, and Dan Ding for instructing and assisting us with the use of the conductivity measuring equipment. Also, I want to acknowledge the Geological Society of America for the grant which supported part of my research costs for field sampling and travel. Finally, I want to thank my family and friends, particularly my wife, Amanda, for all their support and encouragement, without which I would not have been able to accomplish all that I have.

TABLE OF CONTENTS

LIST OF ILLUSTRATIONS

Abstract

CO_2 sequestration in deep saline aquifers has been assessed and in some cases implemented in pilot phases in basins throughout the United States, including the Michigan, Illinois, Williston, and Ohio River basins among others (Smith et al, 2005; Sorensen et al, 2005; Barnes et al, 2009). However, many smaller basins not yet considered may offer significant contributions in storage capacity for CO_2 injection. One such is the Forest City Basin, a shallow, intracratonic basin located in parts of Missouri, Kansas, Iowa and Nebraska. The purpose of this research was to perform a preliminary assessment of the stratigraphy, storage capacity, hydrology, and mineralogy of this basin to determine its suitability and structural trapping capacity for carbon sequestration. The basin is stratigraphically ideal in that it contains the St. Peter Sandstone, a high permeability aquifer at depth, which is overlain by multiple low permeability units that should act as a structural seal for injected CO_2. Stratigraphic reconstruction of the basin shows capacity estimates ranging from <1 to 834 megatonnes CO_2; a significant volume in the context of typical coal-fired power plants which emit approximately 1 megatonne CO_2 annually. Groundwater modeling results highlight potential areas of flow stagnation and a predominately lateral flow regime within the St. Peter Sandstone. This, coupled with relatively low flow velocities in most model scenarios, indicates that CO_2 as a dissolved phase in groundwater is not likely to escape the basin in less than 1,000 years, the commonly accepted performance standard for sequestration (Hepple and Benson, 2005). Mineralogical analysis of the St. Peter indicate a grain matrix composed almost entirely of quartz, suggesting that dissolution of minerals is not likely to occur and

negatively impact pore space connectivity. This analysis is only a first step in considering this basin for CO_2 injection, but results indicate that the Forest City Basin is indeed suitable for carbon sequestration and warrants further investigation.

Introduction

Deep saline aquifers are considered one of the leading candidates for large-scale CO_2 sequestration as they are widespread, are commonly located near major point sources of CO_2, and have high potential CO_2 storage capacity (Bergman and Winter, 1995; Baines and Worden, 2004; Ide et al., 2007; Benson and Cole, 2008; Kopp et al., 2009a,b). Many saline aquifers are also deep enough to have pressures above 7.38 MPa and temperatures above 31° C for CO_2 to exist in a super-critical state in which its density is much greater than in the gaseous state, allowing CO_2 to be stored more efficiently, i.e. requiring much lower pore volume per unit mass of CO_2. The decreased buoyancy of super-critical versus gaseous CO_2 also reduces its ability to leak to the ground surface and enter the atmosphere.

The Forest City basin of the central US is a relatively shallow intracratonic sedimentary basin that to date has largely been overlooked with respect to CO_2 sequestration in favor of deeper sedimentary basins in the region such as the Michigan, Illinois, and Williston Basins (Smith et al, 2005; Sorensen et al, 2005; Barnes et al, 2009). However, based on published stratigraphic reports (Lee, 1943; Anderson and Wells, 1968; Adler et al., 1971; Watney et al., 1997), the Forest City basin contains a significant volume of a major regional aquifer, the St. Peter Sandstone, much of which lies at sufficient depth for CO_2 to be stored super-critically. The objective of the present study was to assess the potential of the St. Peter Sandstone in the Forest City basin for large-scale CO_2 injection and storage.

This assessment entailed the following components: (1) Determining the pore volume of the St. Peter Sandstone which is deep enough and contains saline enough pore fluid to meet minimum federal salinity requirements for wastewater injection, (2) characterizing the hydrology of the basin to place broad constraints on how any injected CO_2 might be transported in the subsurface, and (3) characterizing the mineralogy of the St. Peter Sandstone to constrain how a CO_2-enriched pore fluid might behave chemically in the subsurface.

Geologic Background

The Forest City Basin is a shallow, Paleozoic intracratonic basin covering approximately 83,000 km^2 in Missouri, Kansas, Iowa and Nebraska (Fig. 1). The basin probably originated during the Middle Ordovician as part of the North Kansas basin, which formed in response to uplift of the Chautauqua arch in southeastern Kansas and southern Missouri (Lee et al., 1948; Merriam, 1963; Anderson and Wells, 1968; Adler et al., 1971). Uplift of the Nemaha anticline during the Early Mississippian to Early Pennsylvanian as a result of the Ouachita orogeny subdivided the North Kansas basin into the Salina basin in the west and the Forest City basin in the east (Adler et al., 1971; Rascoe and Adler, 1983). Erosion of the uplifted Nemaha anticline also appears to have supplied much of the Early Pennsylvanian sediment in the Forest City basin. Strong downward displacement on the east side of faults along the Nemaha anticline formed the Forest City basin's depocenter (the deepest part of the basin) and led to its asymmetric west-east profile. The Ouachita orogeny may also have led to uplift of the Bourbon arch, which separates the Forest City basin from the Cherokee basin to the south (Johnson,

2004). The Forest City basin is bounded on the north by the Thurman-Redfield structural zone, a part of the Mid-Continent rift (Tedesco, 1992).

The hydrostratigraphy of the Forest City basin is summarized in Figure 2. The sedimentary rocks of the basin are underlain predominantly by Precambrian igneous felsic rocks and lesser quartzites. Rocks of Cambrian through Lower Ordovician age have largely been eroded from the deeper parts of the basin as a result of uplift of the Southeast Nebraska arch but are better preserved on the basin's shallower eastern flank which experienced less uplift (Merriam, 1963). Listed in order of decreasing stratigraphic age, these rocks include the Cambrian Lamotte Sandstone, Bonneterre Formation, Elvins Group, Potosi Dolomite, and Eminence Dolomite, and the Lower Ordovician Arbuckle Group (Adler et al., 1971). The term "Arbuckle Group" has been used inconsistently in the literature, with some workers defining the base of the Arbuckle at either the top of the Bonneterre or the top of the Precambrian basement (Cole, 1975). In the Forest City Basin, the Arbuckle group is composed of (in order of decreasing stratigraphic age) the Bonneterre and Eminence dolomites, Gunter sandstone, Vanburn-Gasconade dolomitic sequence and the Roubidoux dolomite (Franseen et al, 2004). Overlying the Arbuckle Group is the Middle Ordovician St. Peter Sandstone, which because of its overall depth of occurrence, thickness, and high regional permeability (up to 400 m/yr) is the best potential reservoir for CO_2 sequestration in the Forest City basin. The St. Peter is a well-sorted arenite that commonly contains more than 99% quartz (Dapples, 1955; Pitman et al., 1997). In the Forest City basin it tends to be fairly thin, with thicknesses typically varying from 10 to 20 meters, thinning to the south and

pinching out near the Bourbon arch (Dapples, 1955). The maximum depth of the St. Peter is about 1000-1100 m near the depocenter of the basin.

The St. Peter Sandstone is overlain by a 30-60 m thick Middle to Late Ordovician sequence of limestone, dolomite, and shale that includes the Plattin Limestone (Platteville Formation), Decorah Shale, and Kimmswick (Viola) Limestone. The Plattin Limestone and Decorah Shale contain abundant green-gray shale interbedded with carbonates (Lee, 1943; Lee et al., 1948; Adler et al., 1971). The Kimmswick Limestone consists of coarsely crystalline carbonate rock, much of which has vuggy porosity and high permeability (Adler et al., 1971). Overlying the Kimmswick Limestone is the Maquoketa Shale, a major regional aquitard across the upper Midwest of the US, with an average thickness of about 25-30 m in the Forest City basin (Lee, 1943). The upper Maquoketa Shale consists predominantly of silty dolomite whereas the lower part consists predominantly of dolomitic shale.

The Maquoketa Shale is overlain by the Silurian-Devonian Hunton Group, which consists predominantly of carbonate rocks and can reach a thickness of up to 170 m in the Forest City basin. Overlying the Hunton Group is the Devonian-Mississippian Chattanooga Shale, a black to gray fissile shale and confining unit that extends across much of the southeastern US and varies in thickness from about 15 to 75 m in the Forest City basin. The Chattanooga Shale is overlain by up to 120 m of Mississippian rocks consisting mostly of limestones, including the Chouteau, Gilmore City, Burlington, Keokuk, Warsaw, Spergen, St. Louis, and Ste. Genevieve Limestones. Above the Mississippian limestones lie 120 to 240 m of Pennsylvanian shale and sandstone with minor limestone and coal that comprise the Cherokee Shale. The overlying Marmaton

Group is also shale and sandstone rich but contains a greater abundance of limestone and is thinner at about 30-45 m. The Marmaton Group is overlain by a package of Missourian age rocks consisting of about 45-60 m of sandstone, shale, and lesser limestone comprising the Bourbon Group, about 90-120 m of predominantly limestone with lesser interbedded shale comprising the Bronson, Kansas City, and Lansing Groups, and up to 60 m of the shale-rich Pedee Group. The remaining Upper Pennsylvanian (Virgilian) and Permian rocks in the basin were treated as a single hydrostratigraphic unit in the modeling. The Douglas Group forms the base of this unit and is sandy near its bottom becoming progressively more shale-rich upward over a total thickness of 30-90 m. Overlying the Douglas Group is the Shawnee Group, which consists of about 75 to 115 m of mostly limestone. The Wabaunsee, Admire, Council Grove, and Chase Groups constitute the remainder of the Pennsylvanian-Permian section in the basin and consist of about 180 to 210 m of shales and coarser clastics interbedded with lesser amounts of limestone.

The Forest City basin has seen modest hydrocarbon production from two principal areas (Ball, 1994). Hydrocarbons were first discovered in the basin in 1860 in the Paola field (Fig. 1) and have been extracted mainly from Pennsylvanian sandstones. Subsequent discoveries were made in the Nemaha anticline, from which about 97% of the basin's hydrocarbon production has come, mainly from Ordovician sandstones in the Arbuckle Group, the Viola Limestone, and Silurian-Devonian dolomites. By 1989, conventional oil and gas reserves in the basin had been largely depleted, with cumulative oil production having reached 2.9 billion barrels and mean estimates of undiscovered technically recoverable conventional oil and gas equaling 140 million barrels and 540

billion cubic feet, respectively (Ball, 1994; US Geological Survey, 1994). Coal reserves in the basin have been estimated to be as high as 43 billion metric tonnes and are located primarily in the Pennsylvanian Cherokee Group (Newell et al., 2004). Much of the coal in the Forest City basin is methane-rich (Bostic et al., 1993), and coal-bed methane resources, in which most of the hydrocarbon interest in the basin currently lies, are estimated to be about one trillion cubic feet (Newell et al., 2004). McIntosh et al. (2008) found that this methane was likely produced by microbial action, and that it is chemically similar to methane found in the nearby Illinois and Michigan basins. The Pennsylvanian coals in the Forest City basin are not suitable targets for CO_2 sequestration by methane-CO_2 exchange, as the coals are too shallow for CO_2 to exist super-critically.

Porosity and Hydraulic Conductivity Determinations

Porosity

The CO_2 sequestration capacity of a reservoir is strongly dependent on its porosity. To date, no porosity data for the St. Peter Sandstone in the Forest City basin appear to have been published. However, outside of the Forest City basin, the porosity of the St. Peter Sandstone has been much better characterized. For example, Kreutzfeld (1982) measured the porosity of the St. Peter Sandstone in the Illinois Basin and found values ranging from 12 to 46%, having a weak negative correlation with depth over an interval of 0 to 1600 meters. Other studies from the Illinois Basin show similar variance in porosity, with ranges from <1% to 30% (Fishman and Pitman, 1994) and <1% to 35% (Brynes and Wilson, 1994). In the latter study, heterogeneity in porosity was attributed to increasing depth of samples, grain sorting, and degree of compaction. In the Michigan

Basin, the St. Peter Sandstone was found to have a porosity ranging from <1% to 20% (Moline et al, 1994; Shepherd et al, 1994).

In order to constrain more strongly the porosity of the St. Peter Sandstone within the Forest City Basin, drill core was sought from the state geological surveys of Kansas, Missouri, Iowa, and Nebraska. Two drill cores that intersected the St. Peter Sandstone were found, one from near the depocenter in eastern Kansas and one from the flank of the basin in southwestern Iowa, and were sampled at depths of 1015 and 615 m, respectively (Table 1). To measure the porosity, the samples were first heated in an oven at 100° C for two weeks in order to evaporate any residual water content. Samples were weighed daily during this period to make sure that their mass had stabilized over time. The samples were then saturated with water in a flexible wall permeameter in the Department of Civil and Environmental Engineering at the University of Missouri—Columbia (MU). The samples were considered to be saturated when the flow rate of water into the sample equaled the flow rate out of the sample and the weight of the sample no longer changed over time. From the difference in the mass of the saturated sample and the oven-dried sample, the density of fresh water, and the volume of the bulk sample, effective porosity values of 15% for the shallower sample and 9% for the deeper sample were calculated (Table 1). These results suggest that the St. Peter Sandstone retains significant porosity at depth in the Forest City basin, though the results do not provide much constraint on the degree of heterogeneity of the porosity.

Hydraulic Conductivity

As for porosity, published hydraulic conductivity data for the St. Peter Sandstone and other pertinent hydrostratigraphic units are available mainly from locations outside

the Forest City basin. Figure 3 shows a compilation of hydraulic conductivity ranges for hydrostratigraphic units occurring in the Forest City basin but measured from locations in the Illinois and Michigan basins. Reported hydraulic conductivity values for each hydrostratigraphic unit vary by several orders of magnitude. This variability may in part result from differences in analytical methods used, where permeameter analyses performed over small sample sizes (Kreutzfeld, 1982; this study) tend to yield lower hydraulic conductivity values, whereas well bore analysis performed over larger samples sizes (Moline et al, 1994) tend to yield higher hydraulic conductivity values. Each of the hydrostratigraphic units is also expected to be naturally heterogeneous due to lithofacies variations and differences in sample depth, which correspond to differences in compaction and cementation. For example, Moline et al (1994) found the hydraulic conductivity of the St. Peter Sandstone in the Michigan basin to correlate strongly with six distinct facies identifiable by multiple geophysical log techniques, including neutron porosity, density, sonic and resistivity logs.

The two drill core samples of the St. Peter Sandstone from the Forest City basin that were analyzed for porosity, as well as four drill core samples from the Arbuckle Group, Maquoketa Shale, the Mississippian limestone sequence, and Marmaton Group (see Table 1) were analyzed for hydraulic conductivity using the same flexible wall permeameter in the MU Department of Civil and Environmental Engineering following standard procedures (ASTM Standard D5084-10, 20120). The permeameter design allowed hydraulic conductivity to be measured only in the longitudinal direction of the cores, so that only vertical hydraulic conductivities (K_v) could be determined. Both vertical and horizontal hydraulic conductivity (K_h) measurements were obtained from

outcrops of the St. Peter Sandstone lying about 250 km east of the Forest City basin margin using a TinyPerm II™ portable air permeameter.

The results of the lab permeameter analyses showed the deeper, lower porosity sample (#5) of the St. Peter Sandstone to have a K_v of 14 m/yr and the shallower, higher porosity sample (#4) to have a K_v of 56 m/yr. K_h values for core samples and outcrop samples of the St. Peter Sandstone measured with the TinyPerm II™ air permeameter were found to have much higher hydraulic conductivity values. K_h values from the air permeameter ranged mainly between 10 and 1000 m/yr, with outliers reaching 30,000 m/yr, significantly higher than the core sample values which were primarily in the range of 10's of meters per year. These results show the hydraulic conductivity of the St. Peter Sandstone to correlate strongly with depth, probably chiefly because of increasing compaction with depth, but perhaps also because of weathering and disaggregation of the rock at the ground surface.

The lab permeameter analyses of the Arbuckle, Maquoketa, Mississippian limestone, and Marmaton samples yielded K_v values orders of magnitude lower than those of the St. Peter Sandstone (Table 1) and support the hypothesis that the St. Peter is the most favorable potential reservoir for CO_2 sequestration in the Forest City basin.

Stratigraphic Reconstruction and CO_2 Storage Capacity Estimation

Figures 4-6 illustrate a hydrostratigraphic model of the Forest City basin constructed using the Groundwater Modeling System (GMS)® software package from well logs obtained from digital archives of the geological surveys of Kansas, Missouri, Iowa, and Nebraska. Figure 4 shows the surface traces of five cross sections shown in Figures 5 and 6, as well as a color map of the elevation of the top of the Arbuckle Group.

Surfaces representing the contacts between hydrogeologic units were generated using a natural neighbor interpolation between drill holes. In some areas of the basin, the interpolations produced spurious crossings and pinch outs of hydrogeologic units. These errors were corrected by assigning thicknesses averaged from the nearest surrounding drill holes. The resulting model agrees well with the observations described in the Geologic Background section above.

From this three dimensional hydrostratigraphic model, the volume of the St. Peter Sandstone lying below a depth of 750 m in the Forest City basin could be calculated, resulting in a value of about 440 km^3 distributed over about the western 59% of the area of the basin.

Salinity of the pore fluids must also be considered in storage capacity estimates, as federal law according to the Safe Drinking Water Act of 1974 requires any aquifer targeted for waste injection to have pore fluid total dissolved solids (TDS) contents of at least 10,000 ppm. Salinity data for the St. Peter Sandstone in the Forest City basin are sparse, but generally are greater than 10,000 ppm (Imes, 1985; Siegel, 1989; Jorgensen et al., 1996). In addition, more abundant salinity data from the immediately underlying petroliferous Arbuckle Group are consistently on the order of tens of thousands of ppm (Jorgensen et al, 1996; Carr et al, 2005), supporting the likelihood of >10,000 ppm pore fluids in the St. Peter.

The CO_2 mass storage capacity (G_{CO2}) of the St. Peter Sandstone was calculated from,

$$G_{CO2} = V_T \phi \rho E \quad (1)$$

where V_T represents the total bulk volume of St. Peter at depths below 750 m, ϕ is the average porosity, ρ is the density of CO_2, and E represents the CO_2 storage efficiency factor. The CO_2 storage efficiency factor is a regional scale term that is intended to account for different physical barriers that inhibit CO_2 from contacting 100 percent of the pore volume in the target reservoir (Koide et al., 1992; van de Meer, 2005; Doughty and Pruess, 2004; Shafeen et al., 2004; Bachu et al., 2007). These include areal, vertical, and microscopic displacement efficiencies, gravity effects, and effective porosity. E values for clastic saline aquifers range from 0.51 to 5.4% over the 10 and 90 percent probability range, respectively (US Department of Energy-National Energy Technology Laboratory, 2008), indicating the fraction of the total pore volume that is available for CO_2 storage.

Because of uncertainties in the values of the parameters in equation (1), G_{CO2} values were calculated based on likely minimum and maximum values of porosity and CO_2 storage efficiency factor. For these calculations, the minimum and maximum values for porosity were 1% and the 15% value determined in the present study, and for CO_2 storage efficiency were 0.51 and 5.4%. For a geothermal gradient of 25°C/km (Newell, 1998) and assuming an average surface temperature of 20° C and hydrostatic pressure, the density of CO_2 at 750 m depth was calculated to be approximately 234 kg/m^3 (Stryjek and Vera, 1986). This led to a range of CO_2 storage capacity masses of 5.3 to 830 megatonnes if the St. Peter Sandstone contained unpotable (≥10,000 ppm TDS) water throughout the Forest City basin. This range represents the absolute maximum and minimum values based on available data. However, the actual storage capacity is more likely to lie toward the higher end of this range than the lower. Porous sandstones tend to have high E values (US Department of Energy-National Energy Technology Laboratory,

2008\), and porosities measured in this study on core samples of the St. Peter are on the high end of the overall range reported in the literature (Fig. 3). Figure 7 contours storage capacity in megatonnes CO_2/km^2 for porosity = 15%, storage efficiency = 4%, and CO_2 density = 234 kg/m^3. The figure suggests that significant volumes of CO_2 could be injected in relatively small areas where the St. Peter is thickest; up to 23,500 tonnes/km^2 in some areas.

Hydrologic Modeling

Model set-up

To begin to understand how any injected CO_2 might behave in the St. Peter Sandstone, a hydrologic model of the Forest City basin was constructed that included variable-density groundwater flow, heat transport, and non-reactive solute transport of the bulk salinity. The injection of CO_2, its transport as either a dissolved or immiscible phase, and its chemical reaction with resident pore fluids and the aquifer matrix were not considered in the present modeling. Nonetheless, the characterization of patterns of groundwater flow and temperature can help anticipate CO_2 transport and physical properties in the basin. For example, how rapidly can groundwater flow laterally through the St. Peter and how soon would it arrive from a CO_2 injection well at the 750 m depth contour for the top of the St. Peter Sandstone beyond which any exsolved CO_2 would be converted to a gaseous state? How much vertical leakage and infiltration of groundwater through the formation could be expected? Do any groundwater flow pathways exist from depth in the basin to the ground surface? Knowledge of groundwater flow direction and rate will indicate the direction and rate of transport of dissolved CO_2, and to a lesser extent of immiscible CO_2, based for example on an analysis like that of Hubbert (1953).

Finally, is advective heat transport great enough to perturb the conductive temperature profile and affect the depth at which CO_2 could exist as a supercritical fluid?

The hydrologic modeling was carried out using a combination of the MODFLOW, MT3DMS, and SEAWAT codes in the GMS™ software package for the basin hydrostratigraphic model shown in Figures 4-6. The three-dimensional hydrostratigraphic model was discretized to form a numerical grid with 51 northeast-southwest-trending nodal columns, 105 northwest-southeast-trending nodal columns, and 10 nodal layers. Of the 47,250 cells in the resulting rectangular block grid, 10,350 cells were deactivated because they lay beyond the boundaries of the basin. The topology of cell layer boundaries was also modified to fit the irregular topology of the hydrostratigraphic layer boundaries. This introduces some numerical error into the finite difference solutions employed by the software as this method is based on regular grid spacing, but is at least partially compensated for by gains in geologic accuracy.

The hydraulic and thermal properties of the nine hydrostratigraphic units considered in the model for the initial base case simulation are shown in Tables 2 and 3. The thermal diffusion coefficient in Table 3 was calculated according to equation (2) below:

$$D_{m\_temp}=k_{Tbulk}/\phi\rho c_{Pfluid} \quad (2)$$

Where D_{m_temp} is the thermal diffusion coefficient, k_{Tbulk} is the bulk thermal conductivity, which is a function of the solid matrix and pore fluid conductivities, ϕ is the average porosity, ρ and c_{Pfluid} are the density and heat capacity of the fluid, respectively (Langevin et al, 2007).

Hydraulic boundary conditions for the base case consisted of specified hydrostatic head along the lateral boundaries of the grid and no-flow along the bottom of the grid. Along the top of grid, hydraulic head was specified to be equal to the ground surface elevation, as determined from the US Geological Survey's National Elevation Dataset (Schneider, 2012) and accessed using the GPS Visualizer™ software. The top of the grid was assigned a specified temperature of 20° C, with initial temperatures for the rest of the grid calculated assuming a geothermal gradient of 25° C/km. Groundwater flow and heat transport calculations were carried out at steady-state. Solute (salinity) transport calculations were transient and assumed an initial seawater salinity of 35,000 ppm within the St. Peter Sandstone and Arbuckle Group, which is the approximate average of the range reported by Jorgensen et al. (1996) and Carr et al. (2005). Salinity at the top of the model grid was set to zero and initially increased linearly with depth to the St. Peter Sandstone. No solute sources were specified in the grid. The bottom boundary of the grid was prescribed as a no solute flux boundary, whereas the remaining boundaries of the grid were open to solute flux.

In addition to a base case simulation, which incorporated the most likely parameter values for the basin, three other simulations were calculated to explore the sensitivity of the model results to uncertainties in model parameters. In order to test for maximum groundwater leakage from the St. Peter Sandstone, a "high permeability scenario" was simulated in which the hydraulic conductivities of all of the hydrostratigraphic units were set to their maximum reported values and the St. Peter Sandstone was considered to be isotropic. A low permeability scenario was also simulated in which the hydraulic conductivities of all of the hydrostratigraphic units in

the basin were set to their minimum reported values. Finally, a scenario was modeled in which the St. Peter Sandstone and Arbuckle-basement unit were prescribed to be underpressured according to the data of Jorgensen et al (1996). The apparent low hydraulic heads in these units were suggested by Jorgensen et al. (1996) to result from the fact that these units are recharged from arid regions to the west in Colorado and New Mexico at a rate lower than the rate at which they discharge groundwater from the basin, with little seepage into the St. Peter or Arbuckle through the overlying confining units. In contrast, the shallower units in the Forest City basin are recharged by the more abundant local precipitation.

Base case scenario results

Figure 8 shows hydraulic head contours and groundwater velocity vectors in the Upper Pennsylvanian-Permian sequence, the uppermost hydrostratigraphic unit, for the base case model scenario. The hydraulic head patterns reflect the local variations in topography, which ranges from elevations of 200 to 440 meters. These local variations in topography lead to numerous small, shallow flow cells, some of which are directed opposite to the large scale topographic gradient.

With increasing depth, hydraulic head patterns increasingly reflect the more regional scale topographic patterns (See Figs. 9 and 10). Figure 9 shows hydraulic head and flow patterns for the Hunton Group, which is at an intermediate depth between the Upper Pennsylvanian and Permian units and the St. Peter Sandstone. Figure 10 shows hydraulic head contours and groundwater velocity vectors for the St. Peter Sandstone. Groundwater velocity within the St. Peter ranges from <0.1 to 4.5 m/yr, with the majority of values less than 2.0 m/yr. (Note that here and throughout the manuscript, groundwater

velocities are reported as average linear velocities.) A southeast-trending tongue of high hydraulic heads extends across the northernmost part of the St. Peter, driving groundwater flow south-southwestward across much of the northern half of the St. Peter in the basin, with a lesser east-northeast component of flow in the north easternmost part of the basin. In the southern part of the basin, groundwater flow through the St. Peter is predominantly east-southeastward. Where the two flow regimes converge, near the center of the basin, groundwater velocities reach minimum values, which could help contain CO_2 in the southwestern part of the basin, which is the most favorable for CO_2 injection because of the high depth and possibly high pore fluid salinity of the St. Peter there.

Figure 11 shows head contours (black lines), velocity vectors and geologic units in cross section. The upper units of the model show the groundwater flow cells generated by variations in topography. The results show little groundwater leakage across the boundaries of the St. Peter Sandstone within the Forest City basin, with flow predominately horizontal. Thus, little CO_2 would be lost from the St. Peter due to groundwater advection, though any CO_2 existing in a separate immiscible phase would have a stronger upward component of flow due to buoyancy.

Figure 12 shows the steady-state temperature profile, the distribution of the St. Peter Sandstone, and the 31° C isotherm along the transect A-A′ (Fig. 4). The temperature profile is primarily conductive as indicated by the primarily linear increase in temperature with depth, with little perturbation of this trend that would be expected from advective heat transport. A possible exception to this pattern is the hot spot located in the deepest part of the profile, which may reflect advective transport of heat from the basin

depocenter to the north (Figs. 4 and 11). Overall, the results indicate that the volume of St. Peter Sandstone predicted to lie at sufficient depth for super-critical CO_2 storage is not significantly affected by the hydrology of the basin.

Case 2: High basin hydraulic conductivity with isotropic St. Peter Sandstone

The purpose of the Case 2 simulation was to investigate a scenario that maximized the possibility of vertical groundwater leakage from the St. Peter Sandstone. The hydraulic conductivity values used for this simulation are at the high end of the ranges shown in Figure 3 and the St. Peter Sandstone was assumed to be isotropic. The other model hydrostratigraphic units were anisotropic as in the base case. Other model parameters were the same as for the base case. Results of this simulation can be seen in Figures 13 and 14. Hydraulic head and groundwater velocity patterns in the uppermost hydrostratigraphic unit are nearly identical to those of the base case and are therefore not shown--head is controlled primarily by local topographic variation and regional patterns are not observed. In the St. Peter, hydraulic heads and velocities are similar to those of the base case (shown in Fig. 11). However, smaller variations in head are better preserved in the isotropic case, which creates a somewhat more varied flow regime for the St. Peter compared to that of the base case, as seen in Figure 13. Despite this, intersections between flow regimes still create apparent zones of flow stagnation, primarily in the central portion of the model.

Both vertical and horizontal groundwater flow velocities in the St. Peter are higher in this second case, resulting from increased conductivity and the introduction of isotropy. The differences, however, are not large enough to cause the temperature field to be altered significantly compared to the base case. Figure 14 contours vertical

velocities within the St. Peter. The distribution of vertical flow in this figure is identical to that seen in the base case--only the values for velocity have changed, increasing by an order of magnitude from the base case results. The maximum vertical flow velocity in the St. Peter is 0.36 m/yr in this case, compared with a maximum value of 0.022 m/yr in the base case. Average vertical flow in the isotropic case is 0.04 m/yr versus an average of 0.005 m/yr for the base case. While vertical flow velocities are increased in this simulation, they are still orders of magnitude less than horizontal flow, which has a maximum value of 10.93 and an average of 1.68 m/yr. Figure 15 shows cross sectional flow from this scenario, which indicates primarily horizontal flow within the St. Peter, likely due to the permeability contrast with the overlying shales.

Case 3: Low basin hydraulic conductivity

The Case 3 simulation used minimum values from the hydraulic conductivity ranges shown in Figure 3 and treated the St. Peter Sandstone as anisotropic as for the base case simulation. Other model parameters were also the same as for the base case simulation. Hydraulic heads and groundwater velocities at the surface remain similar to those found in each of the other cases. Head gradients resulting from topography are not as easily transferred through the very low conductivity units overlying the St. Peter, causing the head gradient to be lower there than in the previous scenarios (see Fig 16). In addition, flow in the southern half of the St. Peter is more uniformly west to east whereas in the previous two cases the direction of flow is more variable, though still predominantly from west to east. Flow velocities in the present scenario are significantly less than in the other two scenarios. In the St. Peter, maximum average linear velocities reach 0.02 m/yr, compared to velocities predominantly on the order of 1's of m/yr in the

other two scenarios. These lower groundwater velocities lead to a more gradual convergence of the northern and southern flow regimes in the St. Peter compared to the other two scenarios, reducing the relative degree of vertical flow there.

Case 4: Underpressured hydraulic heads in the St. Peter Sandstone and Arbuckle Group

The motivation for this final simulation was to investigate the origin and effect of underpressured hydraulic heads in the St. Peter Sandstone and Arbuckle Group reported by Jorgensen et al. (1996) and described in the model set-up section above. In the first instance of this case (4a), vertical boundary nodes above the St. Peter Sandstone were assigned hydrostatic hydraulic head values equal to the elevation of the overlying ground surface, as for the base case scenario. Vertical boundary nodes along the St. Peter and Arbuckle-basement units were assigned underpressured hydraulic head values derived from Jorgensen et al. (1996). . Hydraulic heads along the top of the model remained equal to the ground surface elevation, as for the base case scenario. Other model parameters were also the same as for the base case scenario.

Results from the Case 4a simulation for the St. Peter Sandstone are shown in Figure 17. The results share some characteristics with those of the base case in that two flow fields, one trending overall northwest-southeast and the other trending overall west-east are seen in both cases. However, in the present case, hydraulic heads bulge upward strongly in the interior of the basin relative to the basin boundaries, causing groundwater to flow radially out of the basin along its perimeter. These results suggest that if the Jorgensen et al. (1996) data are correct, then the St. Peter Sandstone in the Forest City basin is transiently underpressured because given enough time for the basin groundwater flow system to reach steady-state, hydraulic heads in the St. Peter would equilibrate to the

higher water table head values in the shallower hydrostratigraphic units in the basin that are sustained by the local recharge.

In the second Case 4 instance (i.e. Case 4b), the model was calibrated to the Jorgensen et al. (1996) data by assigning their hydraulic head data for the Cambro-Ordovician section to the top of St. Peter Sandstone in the model as an internal boundary condition, while leaving the remaining model parameters the same as in Case 4a (Fig. 18). The results bear important similarities to those of the base case scenario in that flow is predominantly from northeast to southwest in the northern portion of the basin and predominantly from west to east in the southern portion. Stagnation zones are also present at the intersection of these flow regimes, and though the range of groundwater velocities in the St. Peter are similar to those of the bas case, overall velocities are lower (<2.0 m/yr) compared to the base case due to a shallower head gradient. Thus, if the Cambro-Ordovican aquifer system in the Forest City basin is indeed underpressured, then this would not appear to have negative implications for CO_2 sequestration as the directions of flow in the underpressured case are broadly similar to those in the base case but the magnitudes of flow are lower, which would prolong CO_2 sequestration in the basin.

St. Peter Sandstone Mineralogical Analysis

The CO_2 storage capacity of the St. Peter Sandstone should also be a function of its reactivity with respect to CO_2-enriched pore fluids. Thus, a further goal of this project was to characterize the modal mineralogy of the St. Peter. Though previous research from outside the Forest City Basin has shown the St. Peter to be predominately a quartz arenite (Dapples, 1955; Pitman et al, 1997), highly reactive minerals could exist in minor

or trace amounts, and particularly if concentrated along pore walls could significantly affect pore fluid composition and subsequent mineral precipitation.

Mineralogical characterizations were performed on two different polished thin sections, one cut from a sample near the basin's northeastern margin at a depth of 615 m, and the other cut from a sample near the depocenter of the Forest City basin at a depth of 1020 m (Table 1; samples 4 and 5, respectively). The characterizations were performed by QEMSCAN® analysis using a Quanta FEG 250 scanning electron microscope (SEM) in the Subsurface Energy Materials and Characterization Lab at Ohio State University. Each thin section was analyzed over a 6×6 mm area at a 2.5 μm raster spacing, which generated a total of 36,000 energy dispersive X-ray spectroscopy (EDS) spectra per thin section. These spectra and their accompanying back scattered electron (BSE) brightnesses were then compared to proprietary reference libraries compiled for a broad array of minerals to map the mineral abundance and porosity within the analyzed area of each thin section. A more detailed description of this procedure can be found in Ayling et al. (2012). Because the epoxy filling the pore space in the thin sections was typically filled with numerous small quartz fragments, the QEMSCAN analyses overestimated the abundance of modal quartz and underestimated the porosity in the samples. These values were corrected through a manual point count of the porosity of the BSE images of the areas of QEMSCAN analysis using a 120 μm raster spacing.

Maps of modal mineral abundances determined from the two QEMSCAN analyses are shown in Figures 19 and 20. The results of the two analyses are in good agreement with previous studies cited above in that the mineralogy of both samples was found to consist predominantly of quartz (about 97%). The next most abundant minerals

in the samples are illite, muscovite, and K-feldspar, which collectively make up about 1% of the mineralogy of each sample but are concentrated along pore walls where they would be the most likely minerals after quartz to react with CO_2-enriched pore fluids. The detected minerals likely to be the most soluble in the presence of a CO_2-enriched fluid are calcite and dolomite, but they were found to account only for between 0.06 and 0.2% of the mineralogy. Thus, given the predominance and relatively low solubility of quartz, the St. Peter Sandstone would seem to be at relatively low risk of undergoing substantial porosity increases due to dissolution by CO_2-enriched fluid.

The bulk porosities of the samples determined from the QEMSCAN analyses after correction for quartz fragments in the epoxy were 23.4% for the sample from near the depocenter and 15.8% for the sample from near the basin margin. The porosity value obtained for the sample from near the depocenter is significantly larger than the value of 9% obtained from the permeameter experiment, whereas for the shallower sample from near the basin margin the QEMSCAN porosity value agrees closely with the permeameter value of 15%. Given the small area (6×6 mm) of the QEMSCAN analysis, the permeameter analysis, which was performed over a much larger region (radius of 7.4 cm and length of 14.1 cm), probably reflects more accurately the average porosity of the St. Peter at that sample location.

Discussion

The results of this study show that the St. Peter Sandstone in the Forest City basin has significant potential capacity for CO_2 sequestration. Although the Forest City basin is relatively shallow, approximately 59% of the St. Peter Sandstone in the basin was found to lie below the 750 m depth threshold for CO_2 to exist in a super-critical state.

Salinity data for the St. Peter in the basin are sparse, but they indicate that salinity in the St. Peter probably exceeds 10,000 mg/L throughout most if not all of the basin (Imes, 1985; Siegel, 1989; Jorgensen et al., 1996), so that salinity is unlikely to be a significant limiting factor for CO_2 sequestration. If the average porosity and CO_2 storage efficiency factor for the St. Peter are near the upper end of their ranges of 1 to 15% and 0.51 to 5.4%, respectively, then the St. Peter could sequester hundreds of megatonnes of CO_2, up to 834 megatonnes for the maximum porosity and efficiency factor values, which results in up to 23,500 tonnes per square kilometer of land surface area. Annual CO_2 emissions from electric power generation in the four states that overlap the Forest City basin range from about 23 megatonnes for Nebraska, 35 megatonnes for Kansas, 40 megatonnes for Iowa, to about 75 megatonnes for Missouri (US Environmental Protection Agency, 2012). Thus, the St. Peter Sandstone in the Forest City basin could potentially sequester a significant fraction of these emissions for decadal time scales. Significant additional CO_2 sequestration capacity in the Forest City basin probably also exists in the underlying Arbuckle Formation, up to about 200,000 tonnes per km^2 (Carr et al., 2005).

The hydrogeology of the Forest City basin appears to be favorable for long-term CO_2 sequestration in the St. Peter Sandstone. The St. Peter is overlain by at least four major aquitards, the Decorah and Maquoketa Shales and the Cherokee and Hunton Groups (Fig. 2), which would impede the ascent of CO_2-rich fluids. The strongly horizontal nature of flow in the St. Peter and overlying units and absence of any strong upflow zones would further impede the ascent of CO_2-rich fluids, whether in aqueous solution or as a separate immiscible phase. A greater concern is the relatively short distance from the basin depocenter to the downstream 750 m depth contour for the top of

the St. Peter. Although the flow velocity of a separate CO_2 phase in a multi-phase context was not calculated in the present study, the single-phase groundwater flow velocities that were calculated provide some constraint on possible CO_2 flow velocities. Because of the approximately 30-fold lower viscosity of CO_2 compared to water at 35° C and 75 bars, the horizontal velocity of CO_2 would be at most 30 times faster than that calculated for single-phase groundwater under the same pressure gradient, though in reality CO_2 flow would be slowed by relative permeability and capillary effects. Average linear groundwater velocities in the St. Peter were calculated to be for the most part less than about 2 m/yr, which means that CO_2 velocities would be less than about 60 m/yr. This means that under optimal conditions (i.e. maximum permeability and CO_2 saturated pore space), CO_2 injected near the depocenter could travel approximately 50 km to the 750 m depth contour for the top of the St. Peter to the east in as little as several hundred years. Beyond this distance the CO_2 would be expected to become gaseous rather than super-critical and much lower masses of CO_2 could be sequestered. However, time scales of several hundred years approach the suggested performance standard of 1000 years suggested for CO_2 sequestration sites (Hepple and Benson, 2005), suggesting that once relative permeability, capillary, and mineral trapping effects are taken into account that this performance standard could be met by the St. Peter Sandstone in the Forest City basin. Thus, quantifying these effects represents a clear need for further research. If CO_2 injection were only eliminated from the parts of the St. Peter in the basin that are less than 50 km upstream from the 750 m depth contour for the top of the St. Peter, then CO_2 storage capacity in the St. Peter in the basin may be reduced by as much as 46%, resulting in a range of 2.85 to 453 megatonnes.

Another important need for further research is the acquisition of pore fluid composition data for the St. Peter Sandstone in the Forest City basin. The quartz-dominant mineralogy of the St. Peter indicates that the rock matrix should not be very reactive with respect to CO_2-enriched pore fluids. However, injected CO_2 could react significantly with solutes in the resident pore fluids. Though this may result in essentially permanent sequestration in the form of mineral precipitation for at least some of the injected CO_2, it could also negatively impact porosity and conductivity by clogging pore space. Limited data published for the northeastern part of the basin (Siegel, 1989) suggest a predominantly Na-Cl composition. However, for TDS contents on the order of 10's of thousands of ppm, other solutes could exist in sufficient concentrations to allow the precipitation of carbonate minerals that would promote long-term CO_2 sequestration but also reduce porosity and permeability.

The Forest City basin is also favorable for CO_2 sequestration with respect to its tectonic setting, accessibility, and maturity. The Forest City basin is located in the tectonically stable interior of the United States suggests where the risk of seismic activity is low (Peterson et al, 2008). Contributing to the basin's low seismic risk and suitability for carbon sequestration is the absence of any known major faults or fractures in the region that might provide a conduit for CO_2 to shallower groundwater systems (Jorgensen et al., 1996). The basin also overlaps or is proximal to several large point sources of CO_2 (US Energy Information Administration, 2012). As for the economic maturity of the basin, the majority of oil and gas reserves within the basin have been depleted (Ball, 1994), and though significant coal reserves remain, these are found predominately in stratigraphic units younger than the St. Peter such as the Pennsylvanian Cherokee Group

(Fig. 2). This implies that sequestration operations would not negatively impact resource production, though production of new resources through enhanced oil and gas recovery methods are unlikely to be a viable option to offset the costs of sequestration.

Conclusions

The Forest City Basin, though shallow compared to other sedimentary basins in the central US, appears to have significant potential for large-scale CO_2 sequestration. The St. Peter Sandstone stands out as a potentially favorable reservoir for CO_2 sequestration in the basin because of its combined high depth, porosity, permeability, pore fluid salinity, and volume, though the Arbuckle Group has also attracted attention for CO_2 sequestration (Carr et al., 2005). The St. Peter Sandstone is overlain by several aquitards that should retard if not prevent the ascent of CO_2-rich fluids into shallower, potable groundwater sources or to the atmosphere. Stratigraphic modeling suggests that CO_2 storage capacity within the St. Peter Sandstone in the basin may well be on the order of 100's of millions of tons, with an areal storage capacity of up to 20,000 tons of CO_2 per square kilometer in parts of the basin.

Hydrologic modeling consistently predicts groundwater to flow predominantly southwestward in the northern part of the basin and predominantly eastward in the southern part of the basin. These flow patterns are largely a function of the overlying surface topography. Groundwater velocities determined from the modeling are much less certain than groundwater flow directions because of large uncertainties in the hydraulic conductivities of all of the basin hydrostratigraphic units, but in the St. Peter Sandstone are unlikely to exceed several meters per year. These results indicate that CO_2 as a dissolved species in groundwater in the St. Peter should be trapped below 750 m depth

within the basin for thousands of years based on meter per year transport rates over distances of at least 10's of kilometers, whereas super-critical CO_2 as a separate immiscible phase is likely to remain for at least several hundred years, and likely longer.

Mineralogical analysis of the St. Peter Sandstone shows it to be composed of about 97% quartz, which should make the St. Peter relatively resistant to dissolution by CO_2-enriched fluids and resultant changes in porosity and permeability. minimize the risk of dissolution of the grain matrix and any resulting loss of storage capacity through the collapse of pore space. However, porosity and permeability could be affected by reactions involving CO_2-enriched fluid and resident pore fluids, the compositions of which currently are not well known.

The present study has served as a reconnaissance of the Forest City basin for CO_2 sequestration based on relatively limited available data. The results suggest significant potential for CO_2 sequestration in the St. Peter Sandstone but with wide (order of magnitude scale) bounds of uncertainty in the mass and duration of sequestration. To reduce this uncertainty, future research should focus on more detailed characterization of the hydrologic properties and pore fluid composition of the St. Peter Sandstone and other major hydrostratigraphic units in the basin.

References

Adler, F., and others. 1971. Future petroleum provinces of the Mid-Continent, Region 7, in: Cram, I. (Ed.), Future petroleum provinces of the United States—their geology and potential, AAPG Memoir, 15, 985-1120.

Anderson, K., Wells, J. 1968. Forest City Basin of Missouri, Kansas, Nebraska and Iowa, AAPG Bull., 52, 264-281.

ASTM Standard D5084-10. 2010. Standard Test Methods for Measurement of Hydraulic Conductivity of Saturated Porous Materials Using a Flexible Wall Permeamter, ASTM International, West Conshohocken, PA, DOI: 10.1520/D5084-10, www.atsm.org

Ayling, B., Rose, P., Petty, S., Zemach, E., Drakos, P. 2012. QEMSCAN (Quantitative Evaluation of Minerals by Scanning Electron Microscopy): Capability and application to fracture characterization in geothermal systems, Proceedings, Thirty-Seventh Workshop on Geothermal Reservoir Engineering, Stanford University, SGP-TR-194.

Bachu, S., et al. 2007. CO_2 storage capacity estimation: Methodology and gaps, International Journal of Greenhouse Gas Control, 4, 430-443.

Ball, M. 1994. Forest City Basin Province, in: Powers, R. (Ed.), Petroleum Exploration Plays and Resource Estimates, 1989, Onshore United States—Region 7. Midcontinent, US Dept. of the Interior Open-File Report 94-24, pp. 61-63.

Baines, S., Worden, R. 2004. Geological storage of carbon dioxide, in: Baines, S., Worden, R. (Eds.), Geological Storage of Carbon Dioxide, Geol. Society of London Special Publication 233, pp. 1-7.

Barnes, A., Bacon, D., Kelley, S. 2009. Geological sequestration of carbon dioxide in the Cambrian Mount Simon Sandstone: Regional storage capacity, site characterization, and large-scale injection feasibility, Michigan Basin, Environmental Geosciences, 16, 163-183.

Benson, S., Cole, D.. 2008. CO_2 Sequestration in deep sedimentary formations. Elements, 4, 325-331.

Bergman, P., Winter, E. 1995. Disposal of carbon dioxide in aquifers in the US, Energy Convers. Mgmt. 36, 523-526.

Bostic, J., Brady, L., Howes, M., Burchett, R., Pierce, B. 1993. Investigation of the coal properties and the potential for coal-bed methane in the Forest City Basin. US Geol. Survey, Open-File Report 93-576.

Bowders, J., Blanco, A., Parra, J. 2003. Characterization of permeability of pavement bases in Missouri Department of Transportation's System, MoDOT, RDT 03-005.

Brynes, A., Wilson, M. 1994. Case history—St. Peter and Mt. Simon Sandstones, Illinois Basin, in: Wilson, M. (Ed.), Reservoir Quality Assessment and Prediction in Clastic Rocks, SEPM Short Course Notes, 30, 385-394.

Carr, T., Merriam, D., Bartley, J. 2005. Use of relational databases to evaluate regional petroleum accumulation, groundwater flow, and CO_2 sequestration in Kansas, AAPG Bull., 89 (12), 1607-1627.

Cole, V. 1975. Subsurface Ordovician-Cambrian rocks in Kansas. Kansas Geol. Survey, Subsurface Geology Series 2.

Conley, C. 1980. Petrology of Arbuckle Group, central Kansas. AAPG Bull., 64(6), 960.

Dapples, E. 1955. General lithofacies relationship of the St. Peter Sandstone and Simpson Group: AAPG Bull., 30, 444-467.

Dott, R., Nadon, G. 1992. Modeling of pressure compartments in the St. Peter Sandstone gas reservoir in the Michigan Basin; Final report, June 1989-December 1992.

Doughty, C., Pruess, K. 2004. Modeling super-critical carbon dioxide injection in heterogeneous porous media, Vadose Zone Journal, 3, 837-847.

Evenson, R. 1989. Depositional, diagenetic, and tectonic influences on permeability and porosity in two Cherokee sandstone reservoirs, Greenwood County, Kansas, University of Kansas Master's Thesis.

Finley, R. 2005. An assessment of geological carbon sequestration options in the Illinois Basin, Illinois State Geol. Survey.

Fishman, N., Pitman, J. 1994. Basin-wide paleofluid flow in Cambro-Ordovician siliciclastic rocks of the Illinois Basin: Diagenetic and geochemical evidence from the Mt. Simon and St. Peter Sandstones, in: Ridgley, J., Drahovzal, J., Keith, B., Kolata, D. (Eds.), Proceedings of the Illinois Basin Energy and Mineral Resources Workshop.

Franseen, E., Byrnes, A., Cansler,J., Steinhauff, D., Carr, T. 2004. The geology of Kansas—Arbuckle Group, Kansas Geol. Survey Current Research in Earth Sciences, Bull. 250(2).

Hepple, R., Benson, S. 2005. Geologic storage of carbon dioxide as a climate change mitigation strategy: Performance requirements and the implications of surface seepage, Environmental Geology, 47, 576-585.

Hiscock, K. 2009. Hydrogeology: Principles and Practice, John Wiley & Sons, New York.

Hubbert, M. 1953. Entrapment of petroleum under hydrodynamic conditions, AAPG Bulletin, 37, 1954-2026.

Ide, S., Jessen, K., Orr Jr., F.. 2007. Storage of CO_2 in saline aquifers: Effects of gravity, viscous, and capillary forces on amount and timing of trapping. International Journal of Greenhouse Gas Control, 1, 481-491.

Imes, J. 1985. The ground-water flow system in northern Missouri with emphasis on the Cambrian-Ordovician aquifer, US Geol. Surv. Prof. Paper 1305.

Jorgensen, D., Helgesen, J., Signor, D., Leonard, R., Imes, J., Christenson, S. 1996. Analysis of regional aquifers in the Central Midwest of the United States in Kansas, Nebraska, and Parts of Arkansas, Colorado, Missouri, New Mexico, Oklahoma, South Dakota, Texas, and Wyoming--Summary, US Geol. Survey Professional Paper 1414-A.

Johnson, T. 2004. Stratigraphy, depositional environments, and coalbed gas potential of Middle Pennsylvanian (Desmoinesian Stage) coals—Bourbon Arch Region, Eastern Kansas. Kansas Geol. Survey, Open-file Report 2004-38.

Koide, H., et al. 1992. Subterranean containment and long-term storage of carbon dioxide in unused aquifers and in depleted natural gas reservoirs, Energy Convers. Mgmt., 33(5-8), 619-626.

Kopp, A., Class, H., Helmig, R. 2009(a). Investigations on CO_2 storage capacity in saline aquifers: Part 1. Dimensional analysis of flow processes and reservoir characteristics, International Journal of Greenhouse Gas Control, 3, 263-276.

Kopp, A., Class, H., Helmig, R. 2009(b). Investigations on CO_2 storage capacity in saline aquifers: Part 2. Estimation of straoge capacity coefficients, International Journal of Greenhouse Gas Control, 3, 277-287.

Kraske, K. 1999. The effect of septic systems on groundwater quality in the Prairie aquigroup and Alexandrian-Maquoketa aquifer, Campton Township, Kane county, Illinois, Northern Illinois University Master's Thesis.

Kreutzfeld, J. 1982. Pore geometry and permeability of the St. Peter Sandstone in the Illinois Basin, University of Toledo Master's Thesis.

Langevin, C., Thorne, D., Dausman, A., Sukop, M., Guo, W. 2007. SEAWAT Version 4: A computer program for simulation of multi-species solute and heat transport. US Geological Survey Techniques and Methods, Book 6, Chapter A22.

Lee, W. 1943. The stratigraphy and structural development of the Forest City Basin in Kansas. Kansas Geol. Survey, Bull. 51.

Lee, W., Leathercock, C., and Botinelly, T. 1948. The stratigraphy and structural development of the Salina Basin of Kansas. Kansas Geol. Survey, Bull. 74.

McIntosh, J., Martini, A., Petsch, S., Huang, R., Nüsslein, K. 2008. Biogeochemistry of the Forest City Basin coalbed methane play, International Journal of Coal Geology, 76, 111-118.

Merriam, D. 1963. The geologic history of Kansas. Kansas Geol. Survey, Bull. 162.

Moline, G., Bahr, J., Drzewiecki, P. 1994. Permeability and porosity estimation by electrofacies determination, in: Ortoleva, P. (Ed.), Basin Compartments and Seals, AAPG Memoir, 61.

Newell, K. 1998. Comparison of maturation data and fluid-inclusion homogenization temperatures to simple thermal models: Implications for thermal history and fluid flow in the Midcontinent, Kansas Geol. Survey, Current Research in Earth Sciences, Bull. 240.

Newell, K., Johnson, T., Brown, W., Lange, J., Carr, T. 2004. Geological and geochemical factors influencing the emerging coalbed gas play in the Cherokee and Forest City Basins in Eastern Kansas, Kansas Geol. Survey, Open-File Report 2004-17.

Peterson, M., Frankel, A., Harmsen, S., Mueller, C., Haller, K., Wheeler, R., Wesson, R., Zeng, Y., Boyd, O., Perkins, D., Luco, N., Field, E., Wills, C., Rukstales, S. 2008. Seismic-hazard maps for the conterminous United States, 2008, US Geol. Survey Scientific Investigations Map 3195.

Pitman, J., Goldhaber, M., Spoetl, C. 1997. Regional diagenetic patterns in the St. Peter Sandstone: implications for brine migration in the Illinois Basin, US Geol. Surv. Bull., 17-18.

Piwinskii, A., Netherton, R. 1977. An experimental investigation of the permeability of Kayenta and St. Peter Sandstones to hypersaline brine in the temperature interval 70 to 90°C at 10.30Mpa confining pressure, University of California Master's Thesis.

Qi, L., Carr, T. 2005. Lithofacies cross sections of the St. Louis Limestone, Big Bow and Sand Arroyo Creek fields, Southwest Kansas, Kansas Geol. Survey, Open-File Report 2005-14.

Ramondetta, P. 1990. El Dorado—An old field with potential, Oil and Gas Journal, March 26, 110-116.

Rascoe, B., Adler, F. 1983. Permo-Carboniferous hydrocarbon accumulations, Midcontinent, USA, AAPG Bull., 67, 979-1001.

Sanders, D. 1959. Sandstones of the Douglas and Pedee Groups in northeastern Kansas, Kansas Geol. Survey Bull., 134(3), 125-159.

Schneider, A. 2012. GPS Visualizer <http://www.gpsvisualizer.com> Accessed 11-11-2012.

Schwartz, F., Zhang, H. 2003. Fundamentals of Ground Water, John Wiley & Sons, New York.

Shafeen, A., Croiset, E., Douglas, P., Chatzis, I. 2004. CO_2 sequestration in Ontario, Canada Part 1: Storage evaluation of potential reservoirs, Energy Convers. Mgmt., 45, 2645-2659.

Shepherd, L., Drzewiecki, P., Bahr, J., Simo, J. 1994. Silica budget for a diagenetic seal, in: Ortoleva, P. (Ed.), Basin Compartments and Seals, AAPG Memoir, 61.

Siegel, D. 1989. Geochemistry of the Cambrian-Ordovician aquifer system in the northern Midwest, United States, US Geol. Survey Professional Paper 1405-D.

Smith, S., Burke, R., Helmd, L., Fischer, D., Sorensen, J., Peck, W., Steadman, E., Harju, J. 2005. Sequestration potential of petroleum reservoirs in the Williston Basin, Plains CO_2 Reduction (PCOR) Partnership Topical Report for US

Sorensen, J., Jensen, M., Steadman, E., Harju, J. 2005. Geologic sequestration potential of the PCOR Partnership region, Plains CO_2 Reduction (PCOR) Partnership Topical Report for US

Spoerl, C. 1983. Modeling of porosity, permeability, and microstructure of the St. Peter Sandstone, University of Wisconsin-Milwaukee Master's Thesis.

Stryjek, R., Vera, J. 1986. PRSV: An improved Peng-Robinson equation of state for pure compounds and mixtures, J. Chem. Eng., 64, 323-340.

Tedesco, S. 1992. Coalbed methane potential assessed in Forest City Basin, Oil and Gas Journal, 68-72.

US Department of Energy - National Energy Technology Laboratory, 2008. Methodology for development of geologic storage estimates for carbon dioxide.

US Energy Information Administration, 2012. State profiles and energy estimates. www.eia.gov/beta/state/

US Environmental Protection Agency, 2012. Inventory of US greenhouse gas emissions and sinks 1990-2010, Washington, D.C., EPA 430-R-12-001.

US Geological Survey. 1994. Petroleum exploration plays and resource estimates, 1989, onshore United States--Region 7, Mid-Continent, Open-File Report 94-24.

Van De Meer, B. 2005. Carbon dioxide storage in natural gas reservoir, Oil & Gas Science and Technology-Rev. IFP, 60 (3), 527-536.

Watney, W., Stephens, B., Newell, K. 1997. Shallowing-upward events and their implications for internal correlations and depositional environment of the St. Peter Sandstone in the Forest City Basin, Northeastern Kansas, Oklahoma Geological Survey Circular, 99, 267-275.

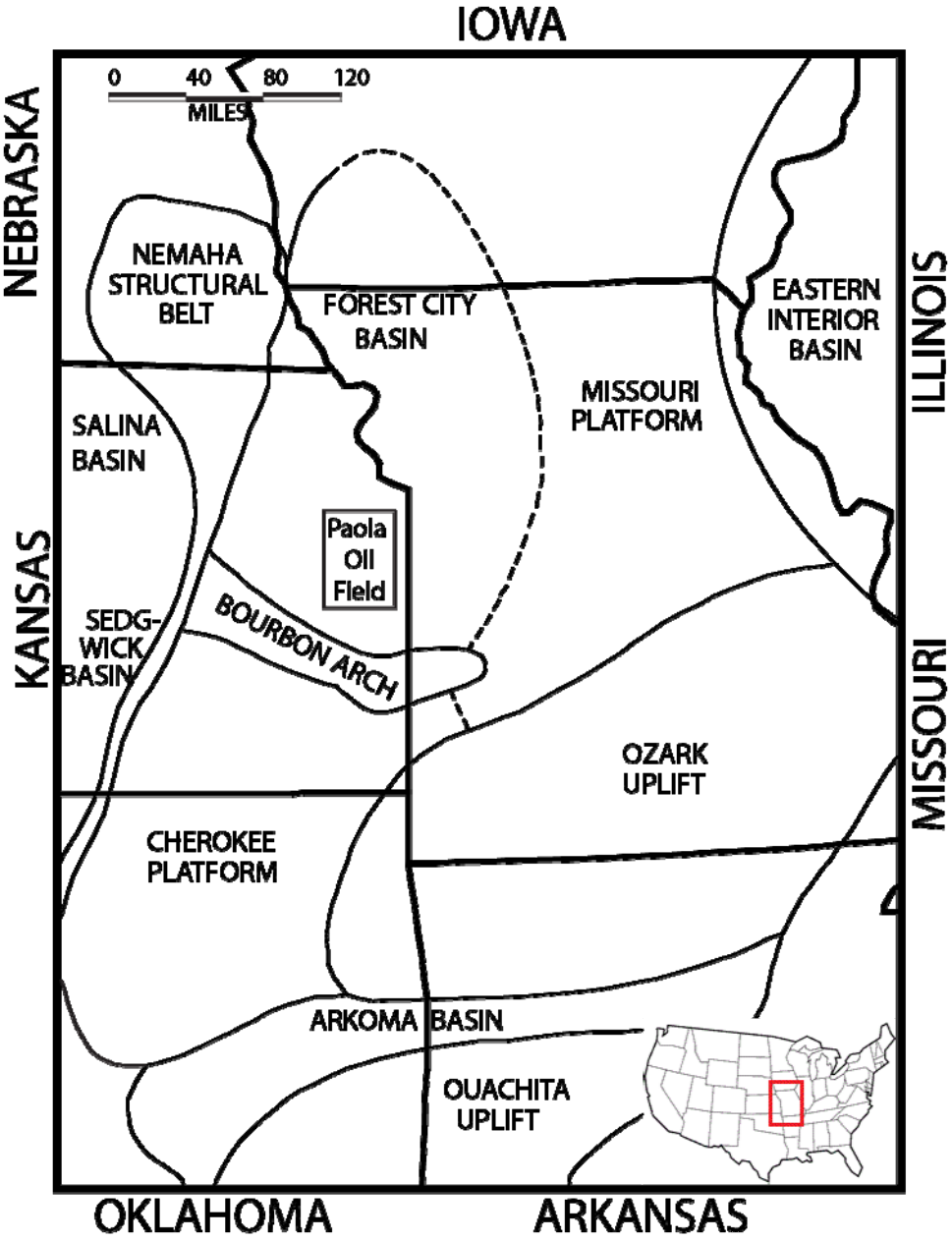

Figure 1: Map of the Forest City Basin after Anderson and Wells (1968)

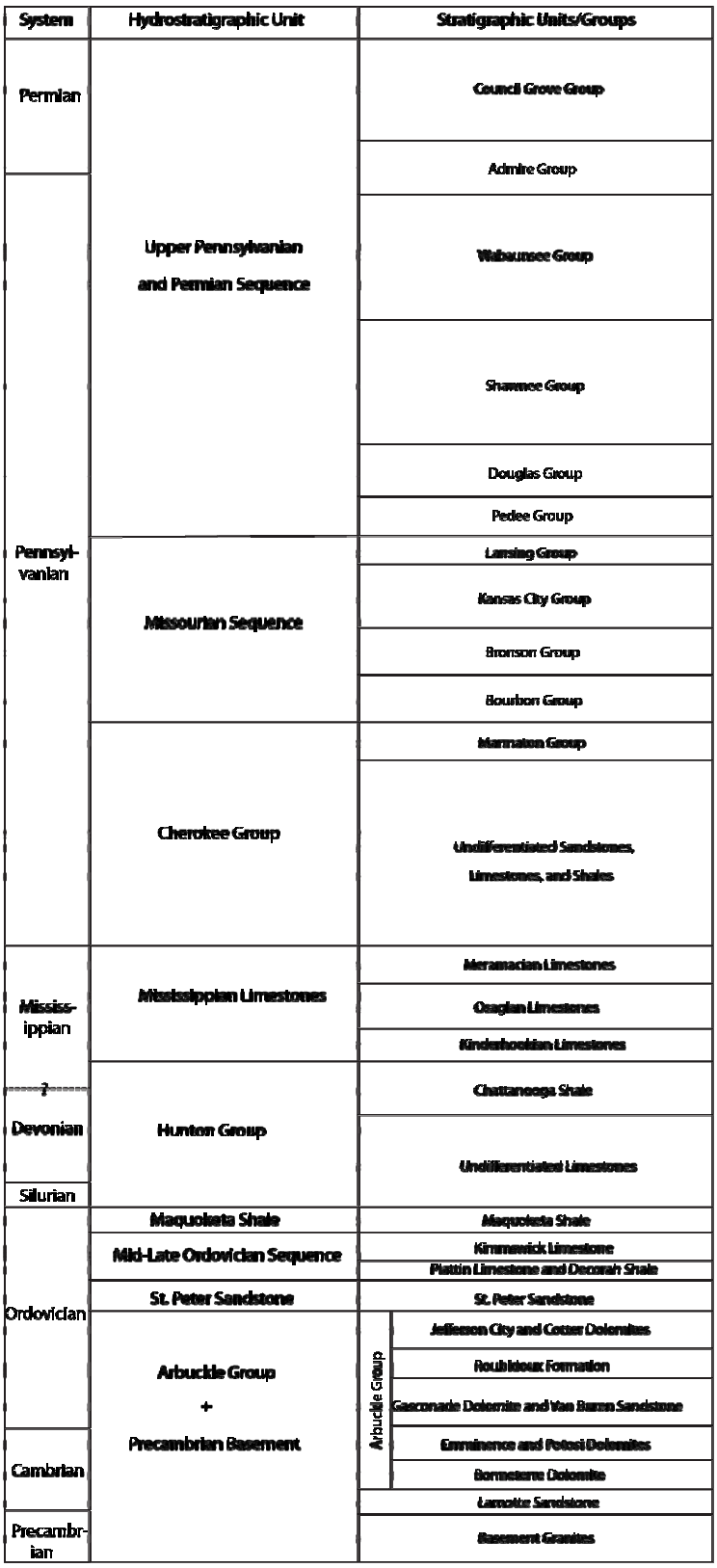

Figure 2: Stratigraphic column of the Forest City Basin after Lee (1943)

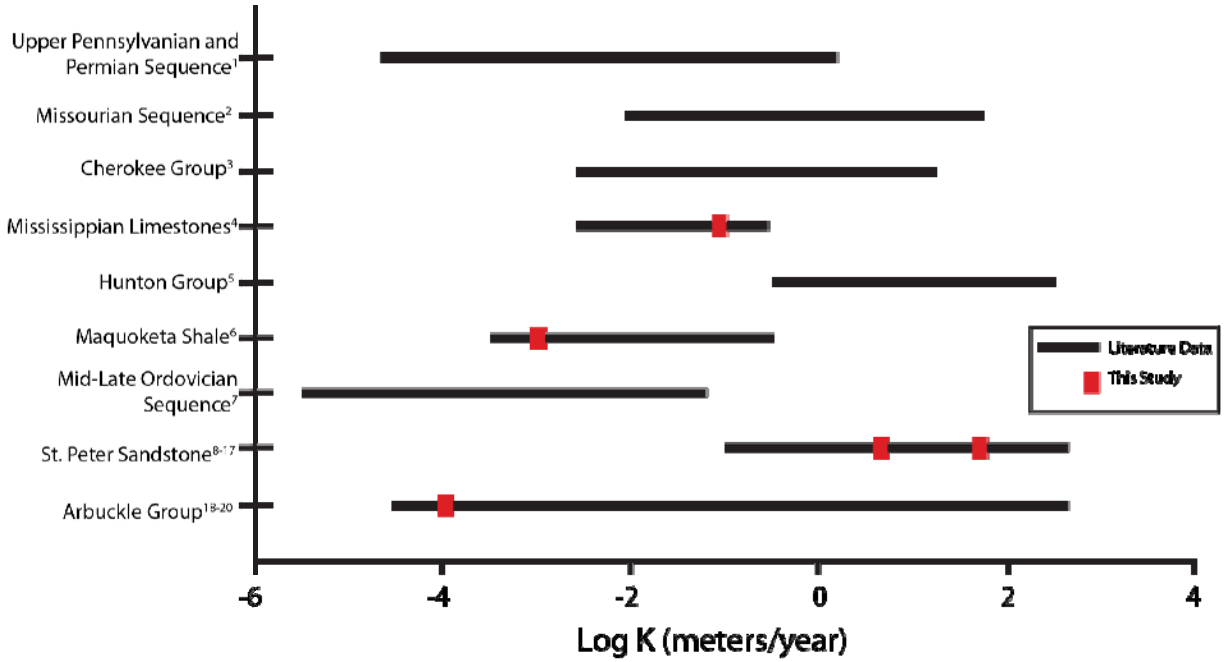

Figure 3: Conductivity ranges from literature sources (black bars) and measured values from this study (red boxes). Sources: [1]Sanders (1959), [2]Byrnes (2000), [3]Evenson (1989), [4]Qi and Carr (2005), [5]Hiscock (2009), [6]Kraske (1999), [7]Schwartz and Zang (2003), [8]Moline et al (1994), [9]Piwinski and Netherton (1977), [10]Spoerl (1983), [11]Kreutzfeld (1982), [12]Finley (2005), [13]Bahr et al (1994), [14]Brynes and Wilson (1994), [15]Shepherd et al (1994), [16]Dott and Nadon (1992), [17]Fishman and Pitman (1994), [18]Ramondetta (1990), [19]Conley (1980), [20]Franseen et al (2004)

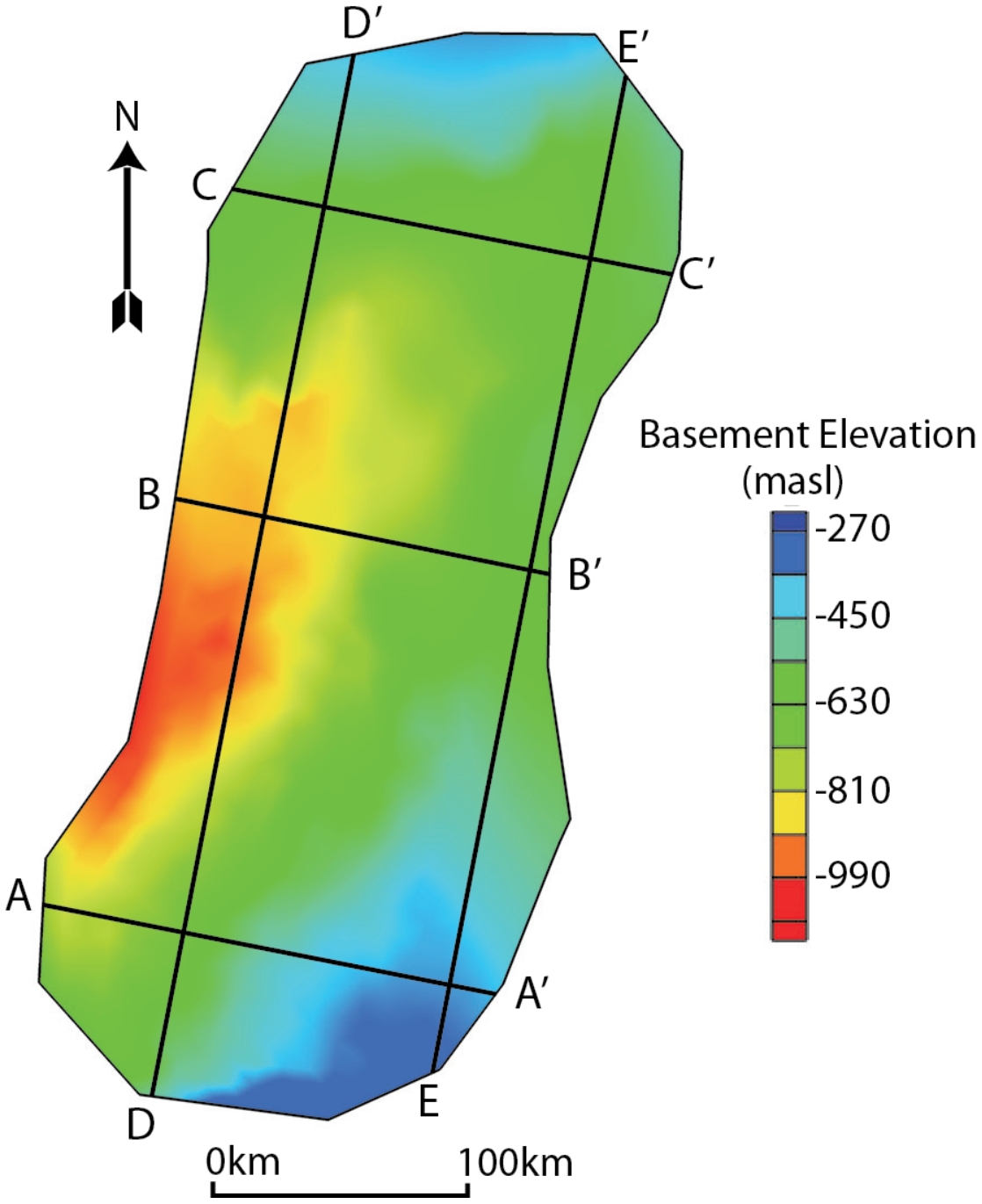

Figure 4: Basin model in plan view contouring basement elevation

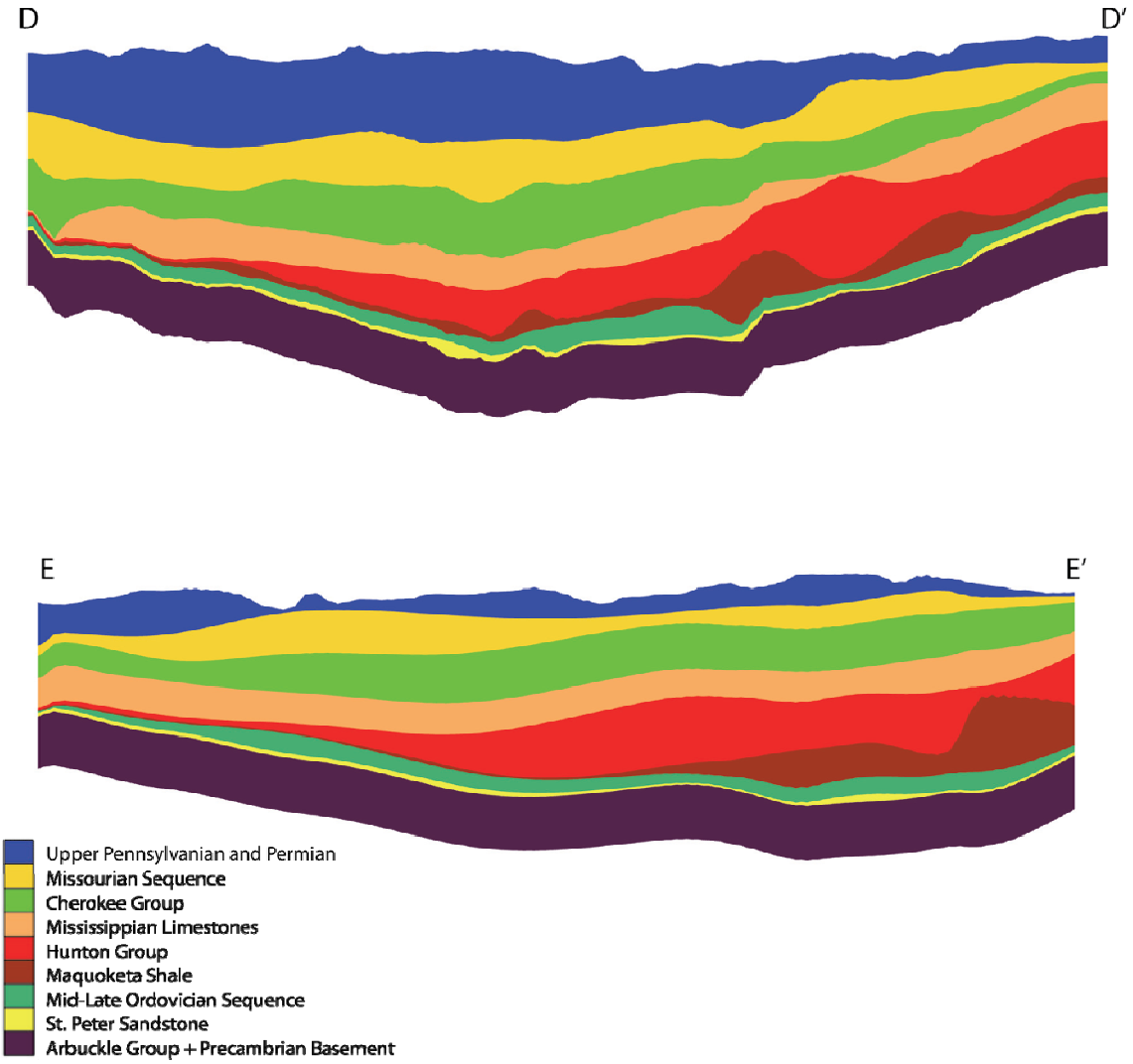

Figure 5: Model-generated NE-SW trending cross sections (see Fig. 4 for locations)

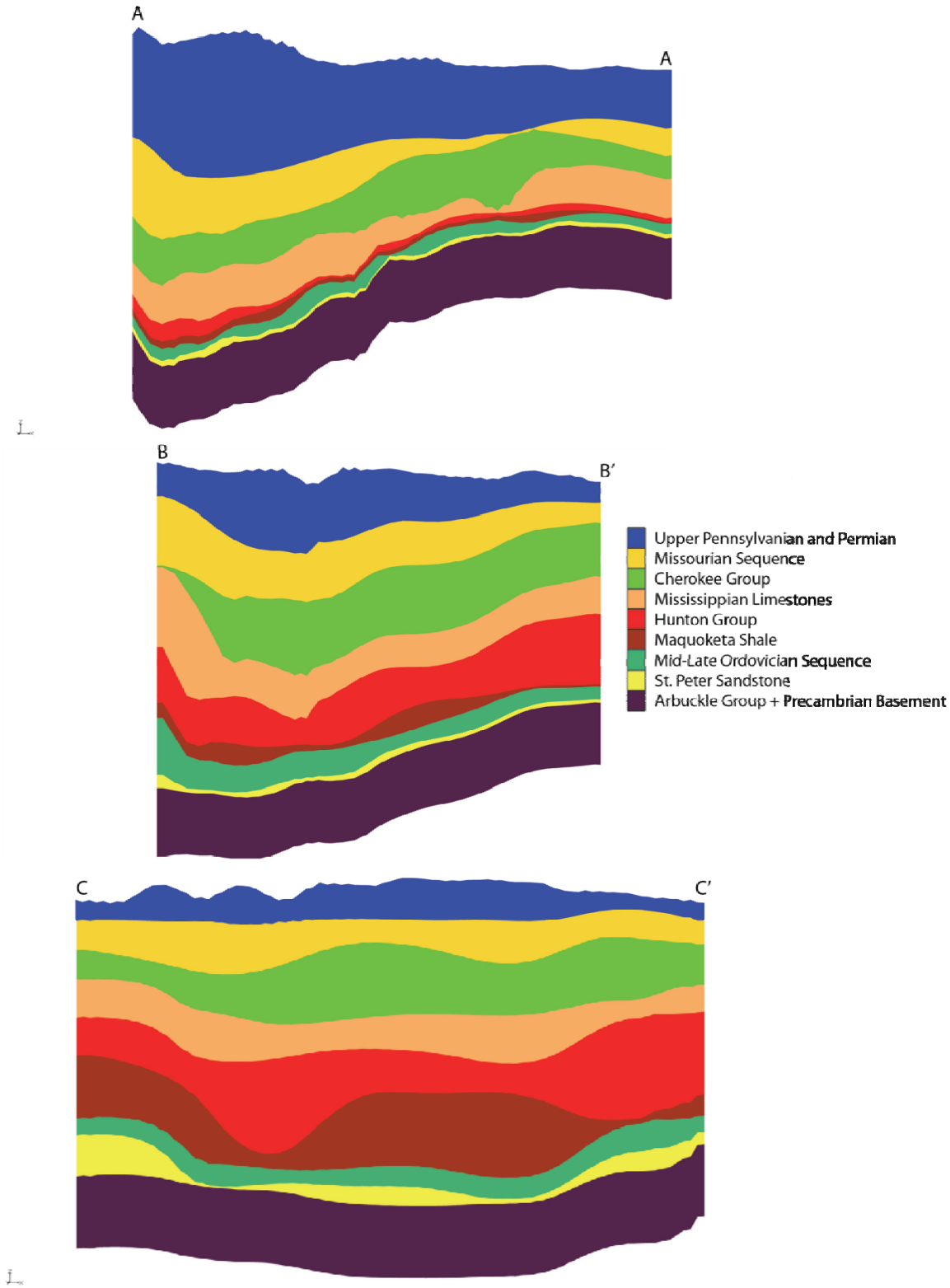

Figure 6: Model-generated WNW-ESE trending cross sections (see Fig. 4 for locations)

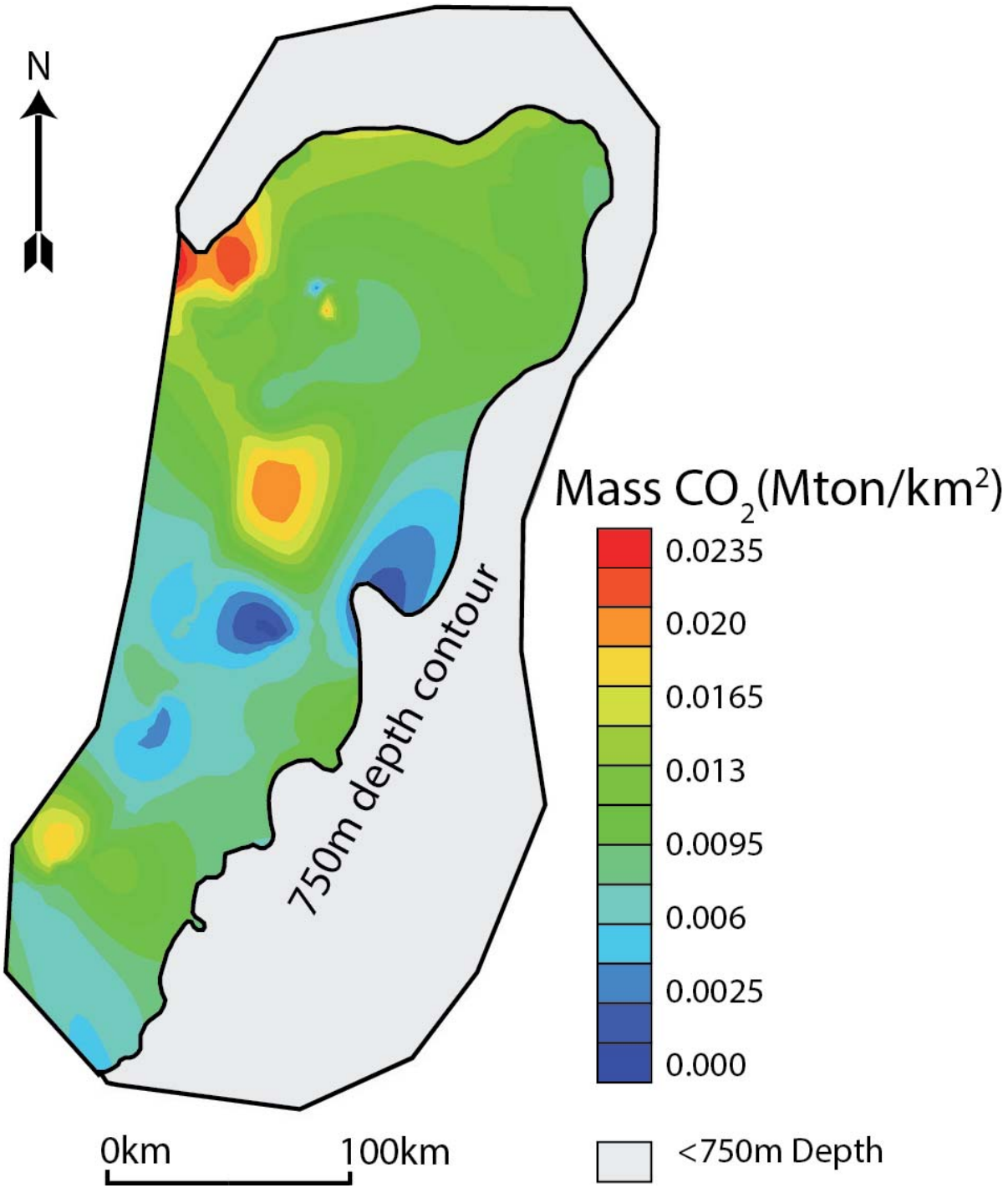

Figure 7: Total storage capacity per km^2 with a porosity of 15%, storage efficiency of 4% and density of CO_2 of 234kg/m^3

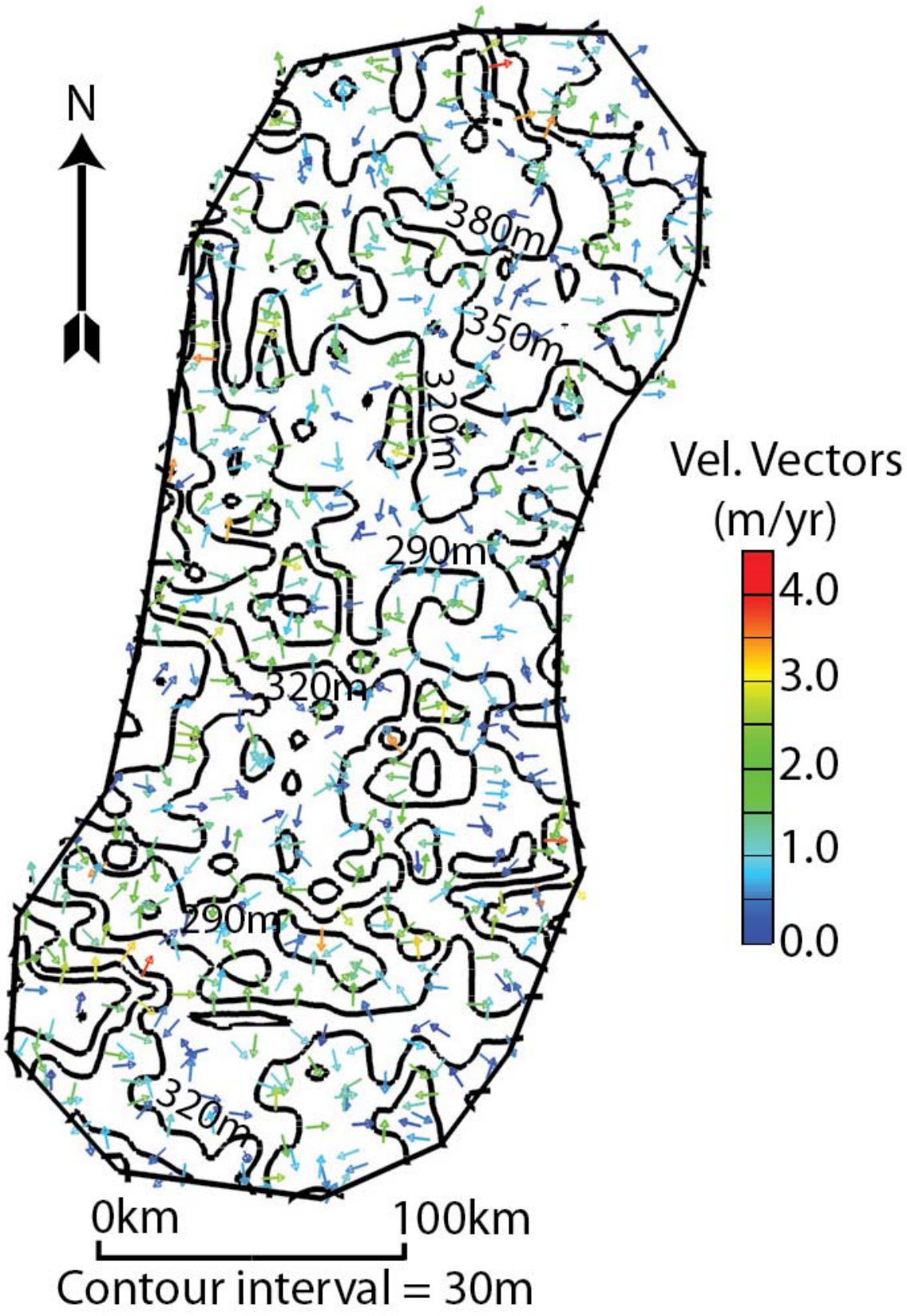

Figure 8: Head contours (black lines) and scaled velocity vectors (colored arrows) for the Upper Pennsylvanian and Permian unit in the base case scenario

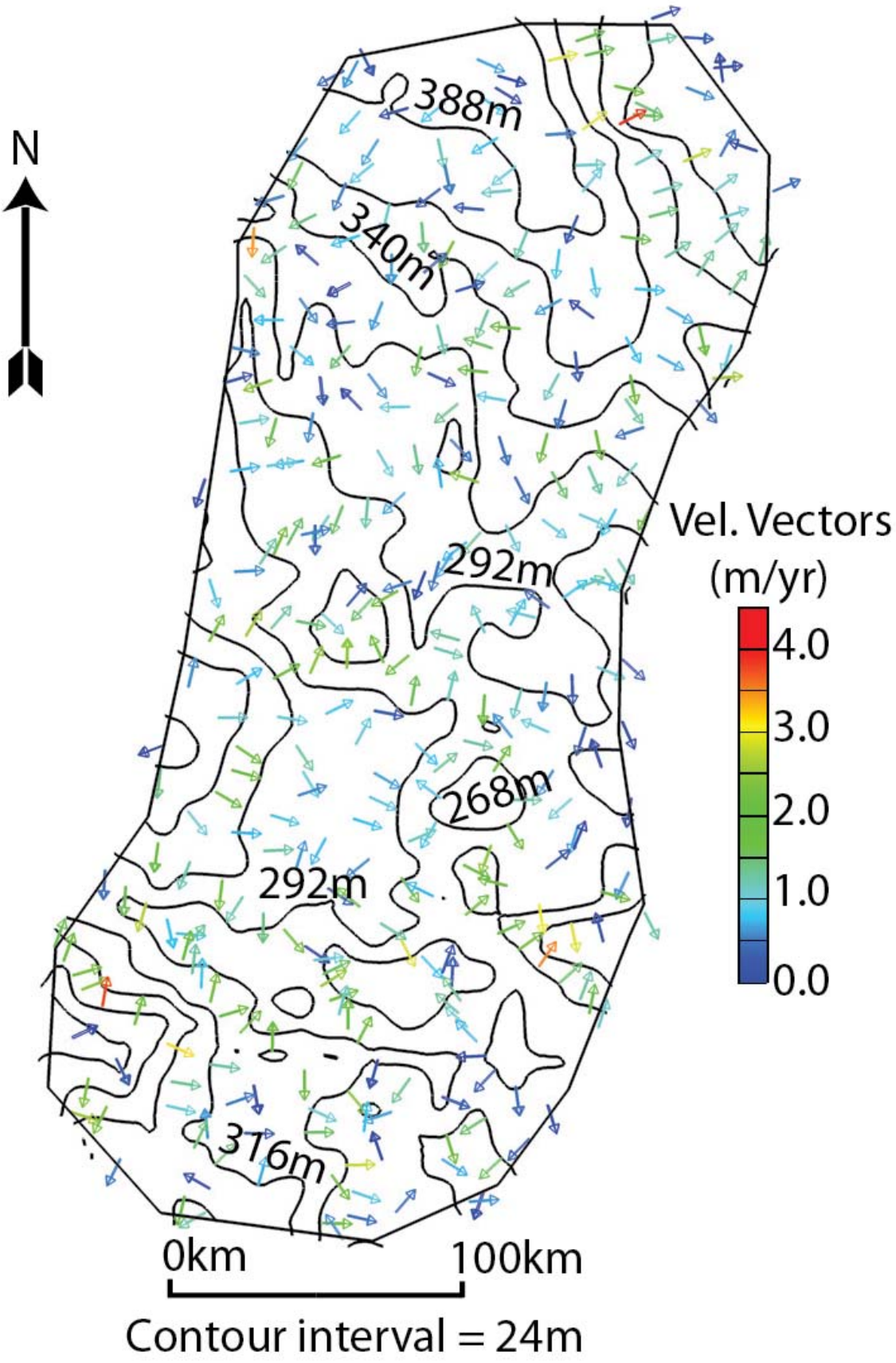

Figure 9: Head contours (black lines) and scaled velocity vectors (colored arrows) for the Hunton Group in the base case scenario

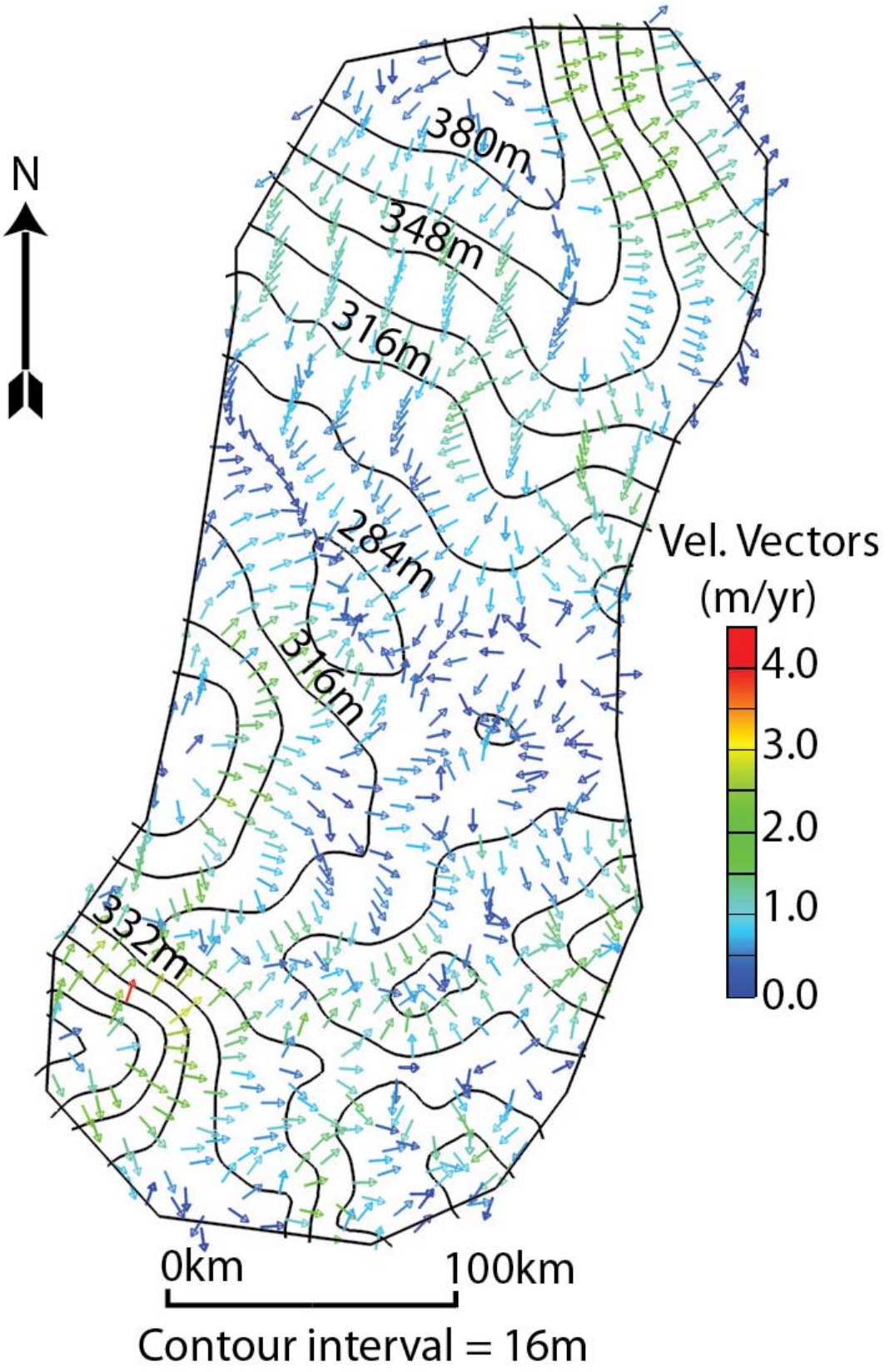

Figure 10: Head contours (black lines) and scaled velocity vectors (colored arrows) for the St. Peter Sandstone in the base case scenario

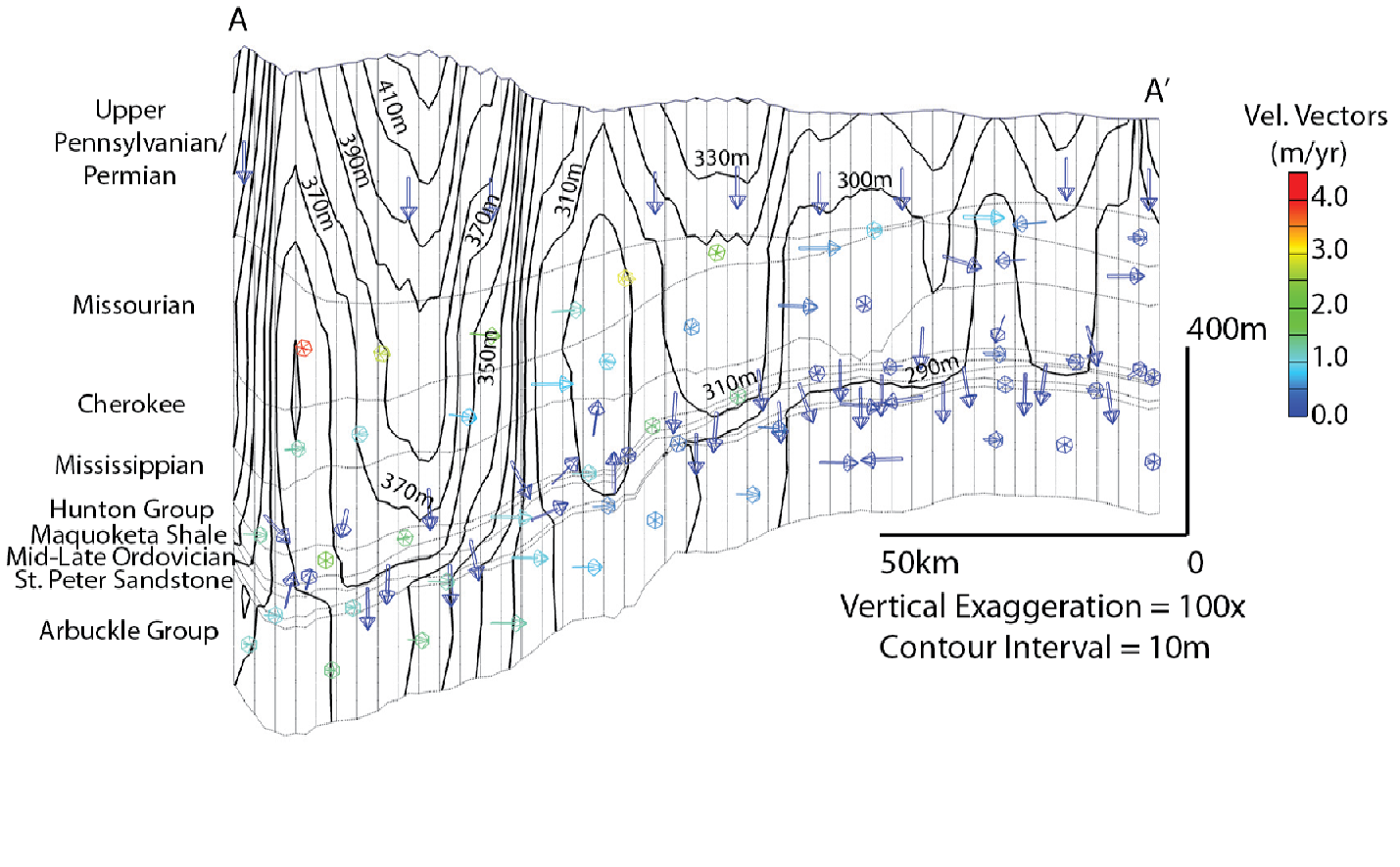

Figure 11: Head contours (black lines) and scaled velocity vectors (colored arrows) along cross section A-A' for the base case scenario

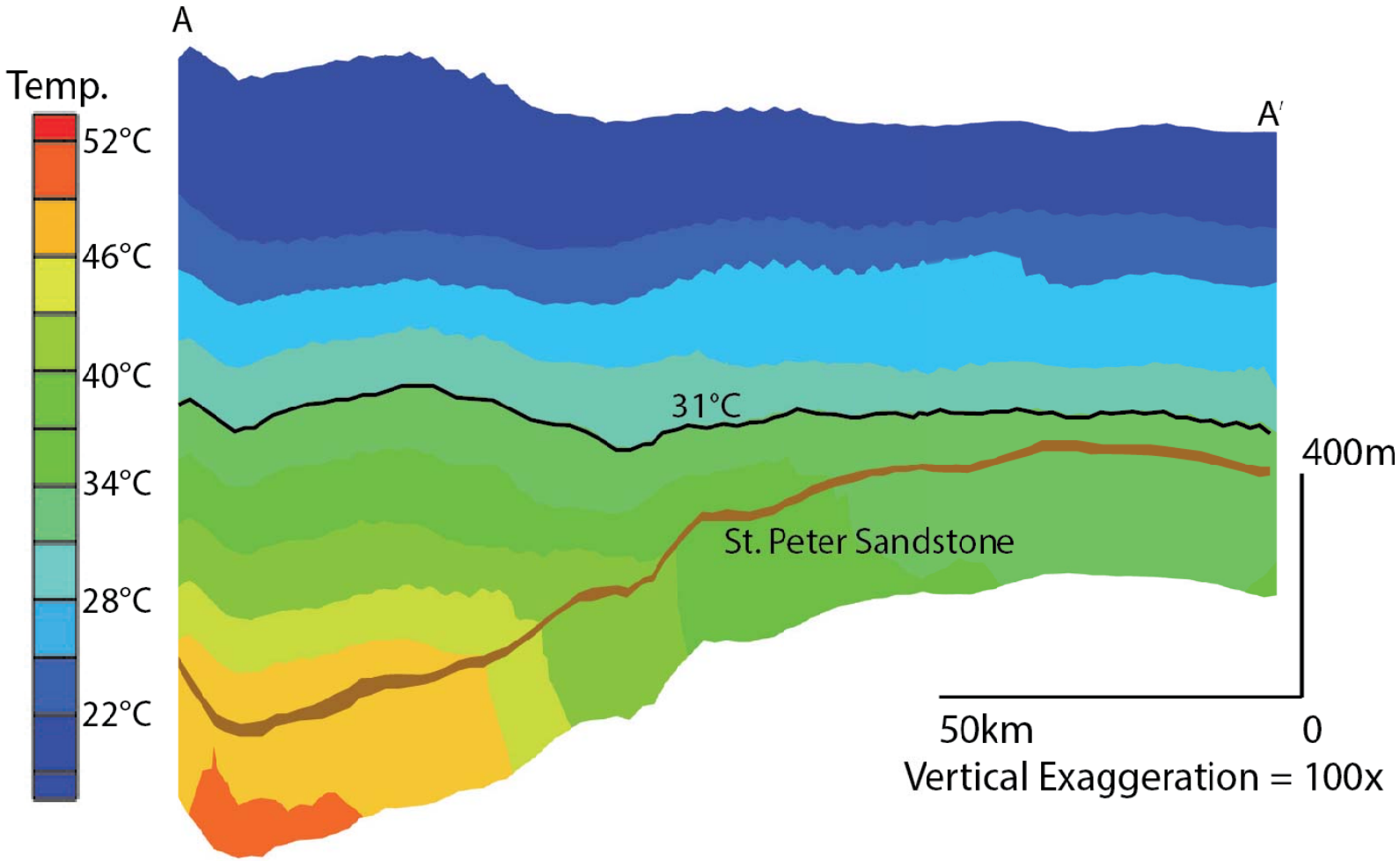

Figure 12: Temperature profile after heat transport simulation along cross section A-A' for the base case scenario

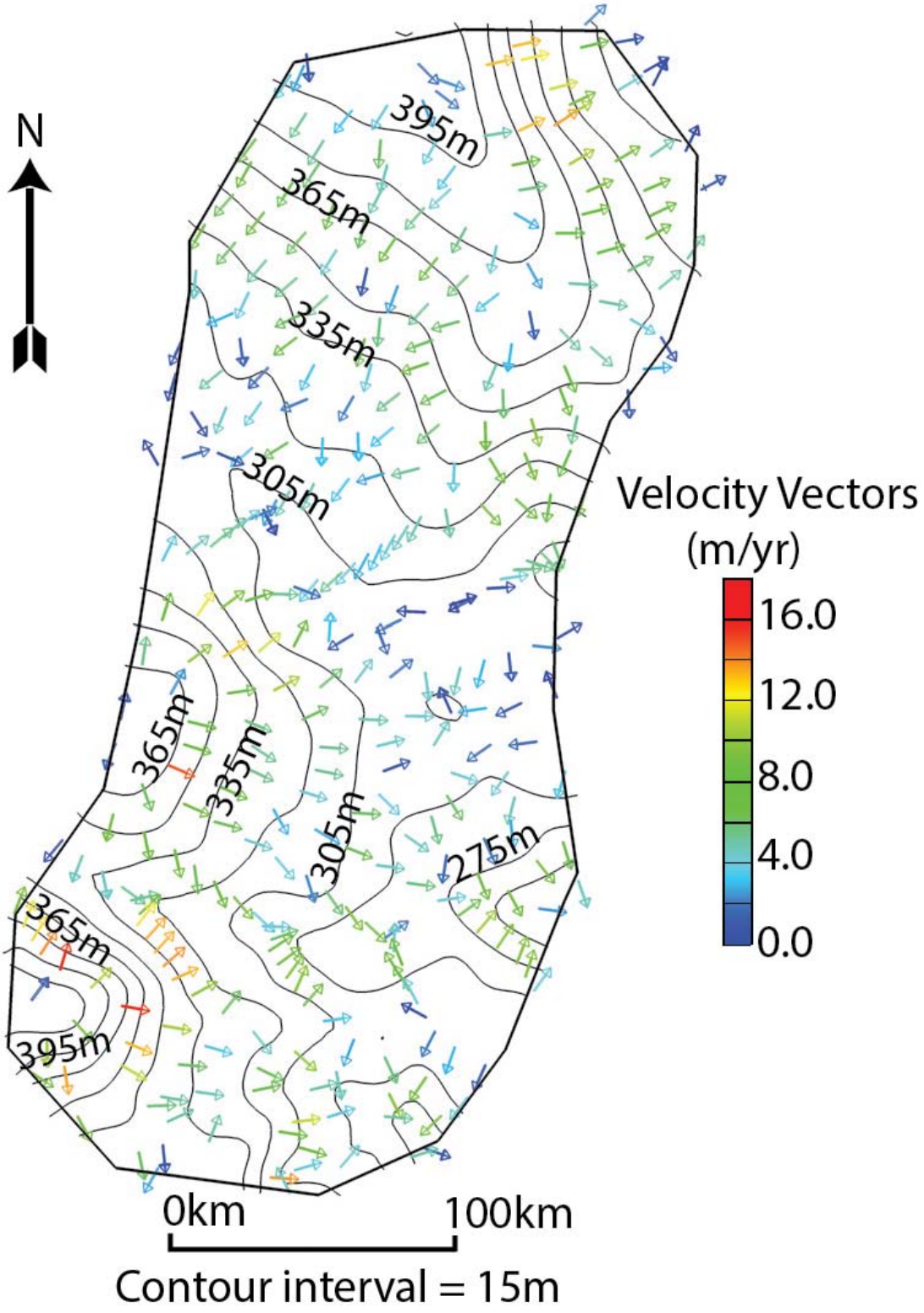

Figure 13: Head contours (black lines) and scaled velocity vectors (colored arrows) for the St. Peter Sandstone for Case 2 (maximum leakage)

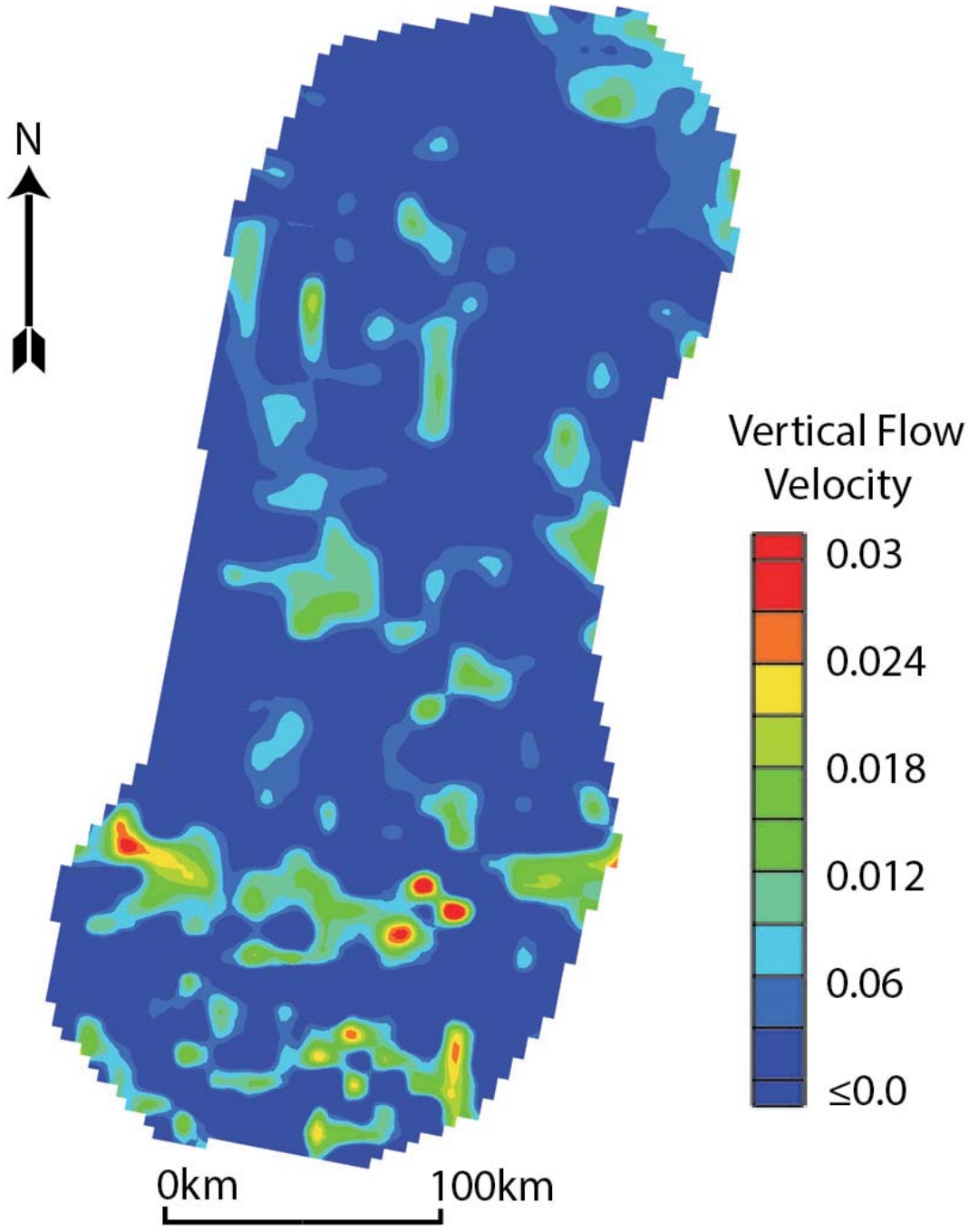

Figure 14: Vertical velocity contours for the St. Peter in Case 2 (maximum leakage). Blue colors represent either no vertical flow or downward flow.

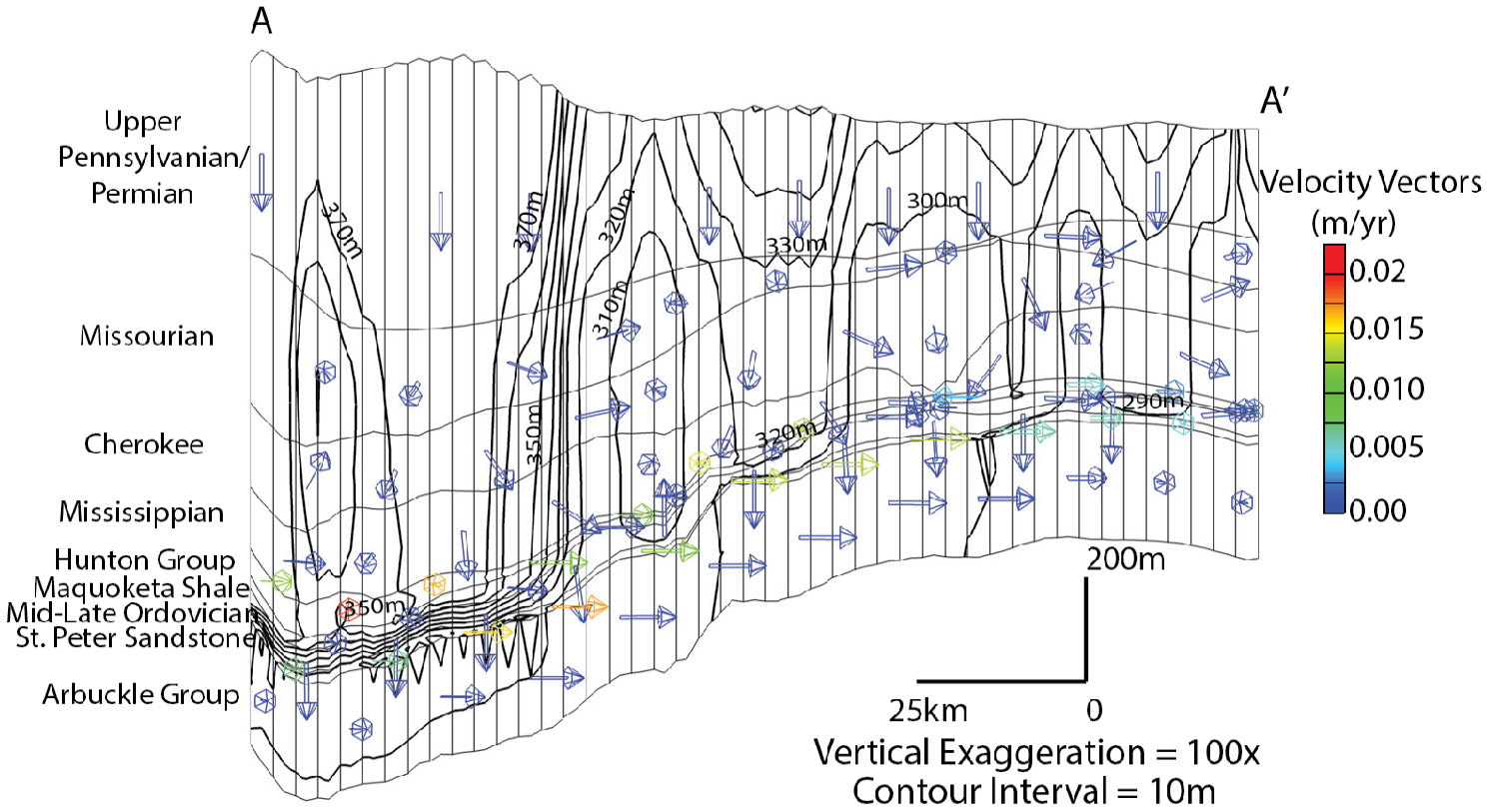

Figure 15: Head contours (black lines) and scaled velocity vectors (colored arrows) along cross section A-A' for Case 2 (maximum leakage)

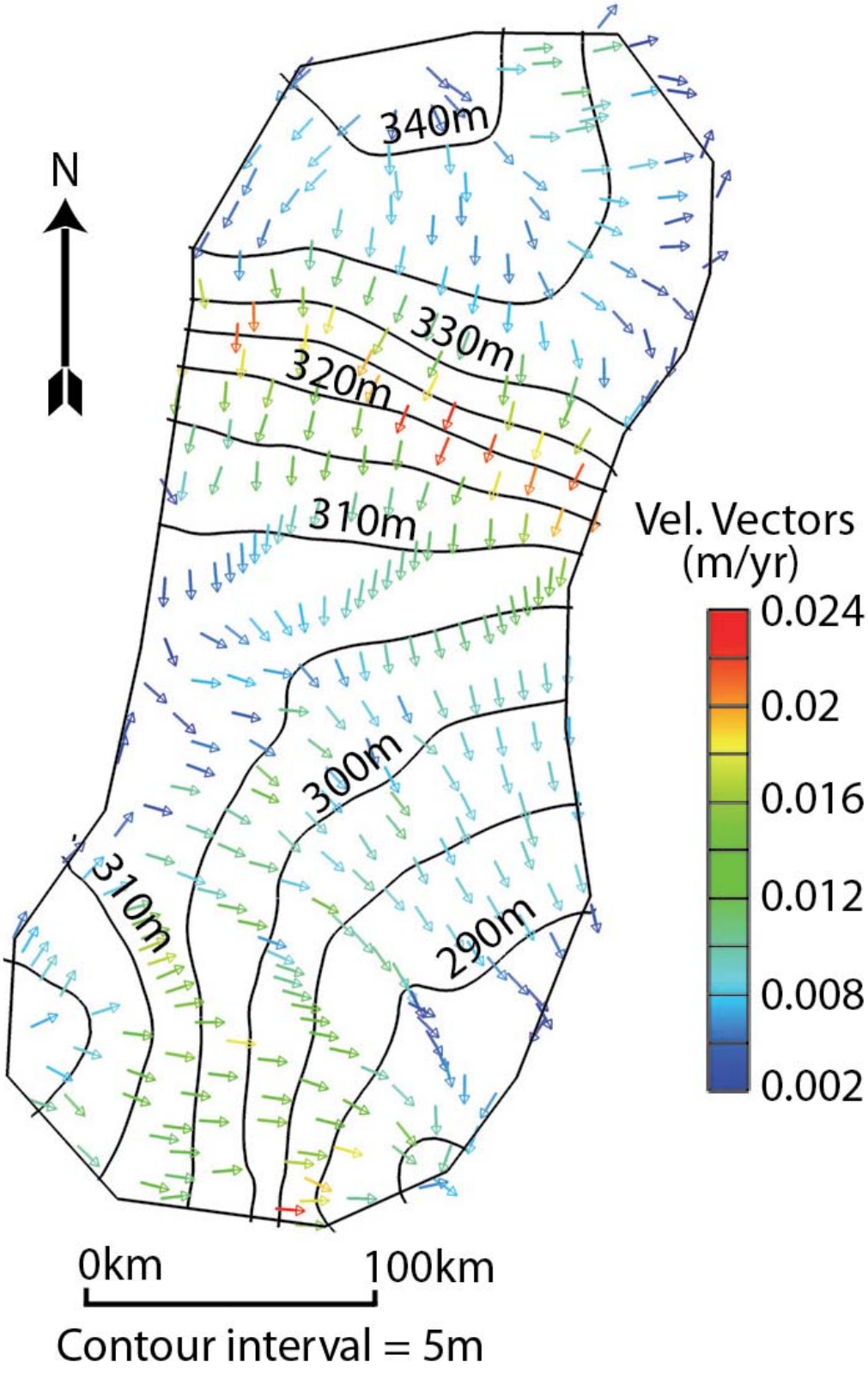

Figure 16: Head contours (black lines) and scaled velocity vectors (colored arrows) for the St. Peter Sandstone in Case 3

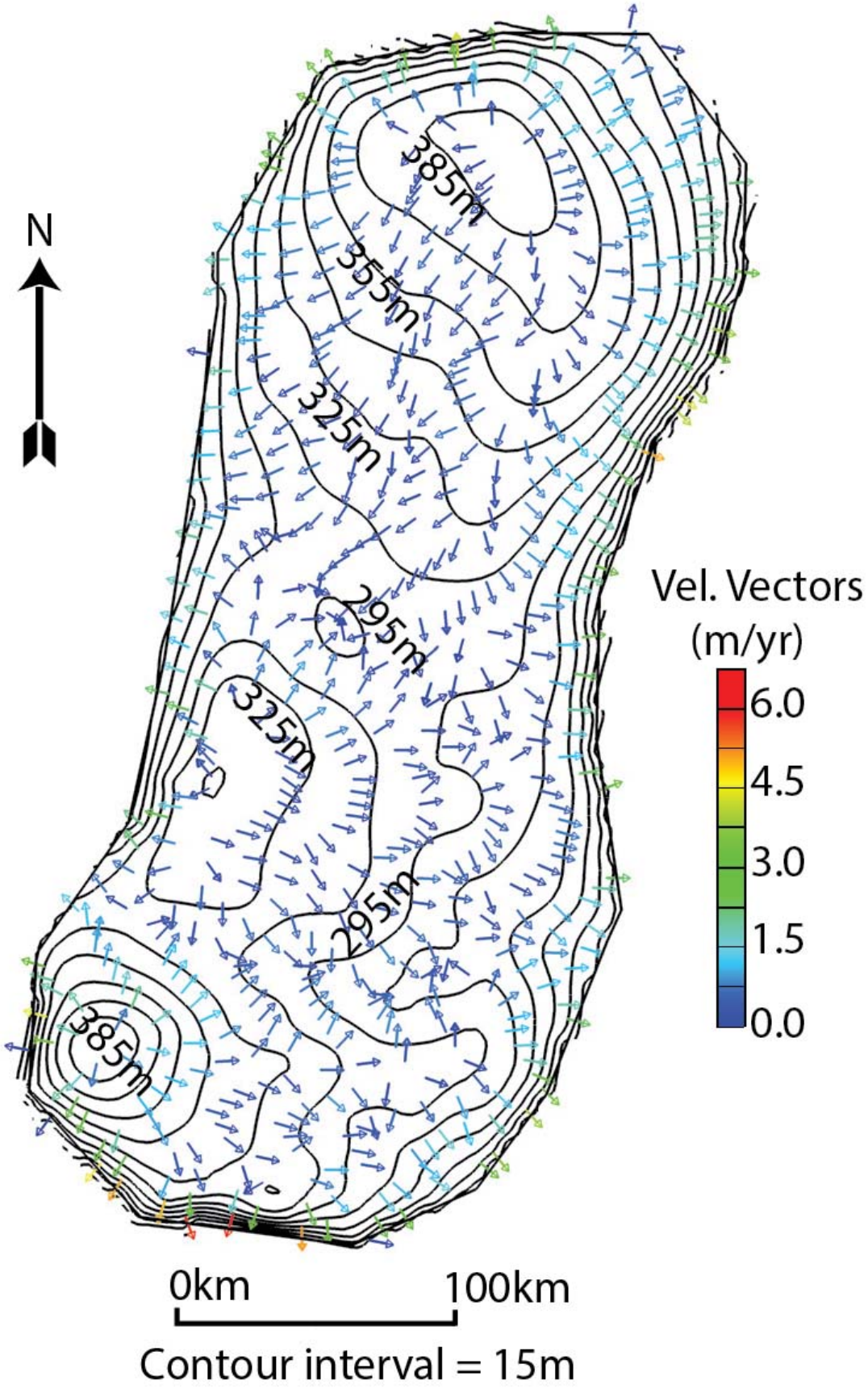

Figure 17: Head contours (black lines) and scaled velocity vectors (colored arrows) for the St. Peter Sandstone in Case 4a

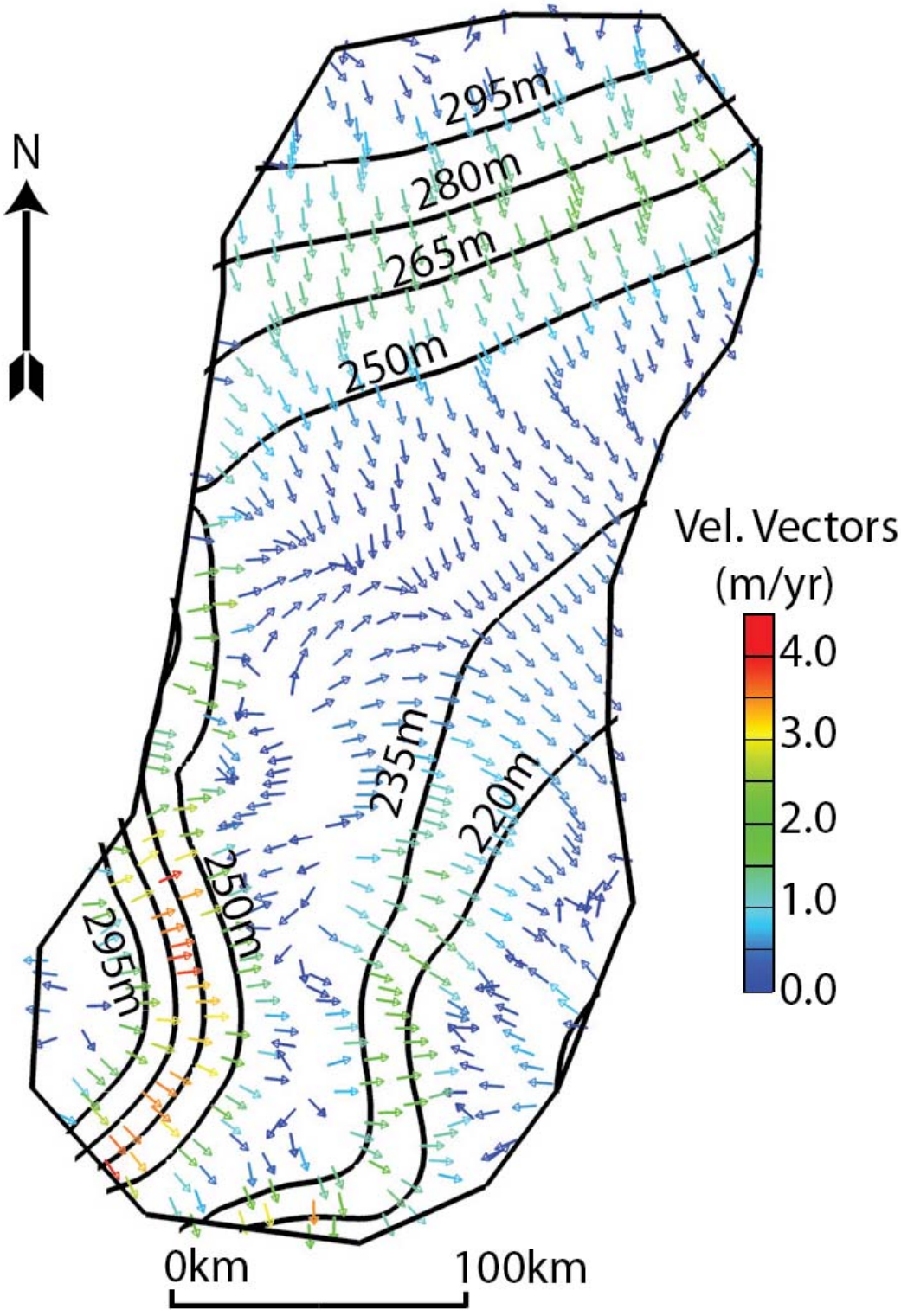

Figure 18: Head contours (black lines) and scaled velocity vectors (colored arrows) for the St. Peter Sandstone in Case 4b (lower heads in Cambro-Ordovician aquifer) with the St. Peter – Mid-Ordovician Group contact assigned constant head boundary

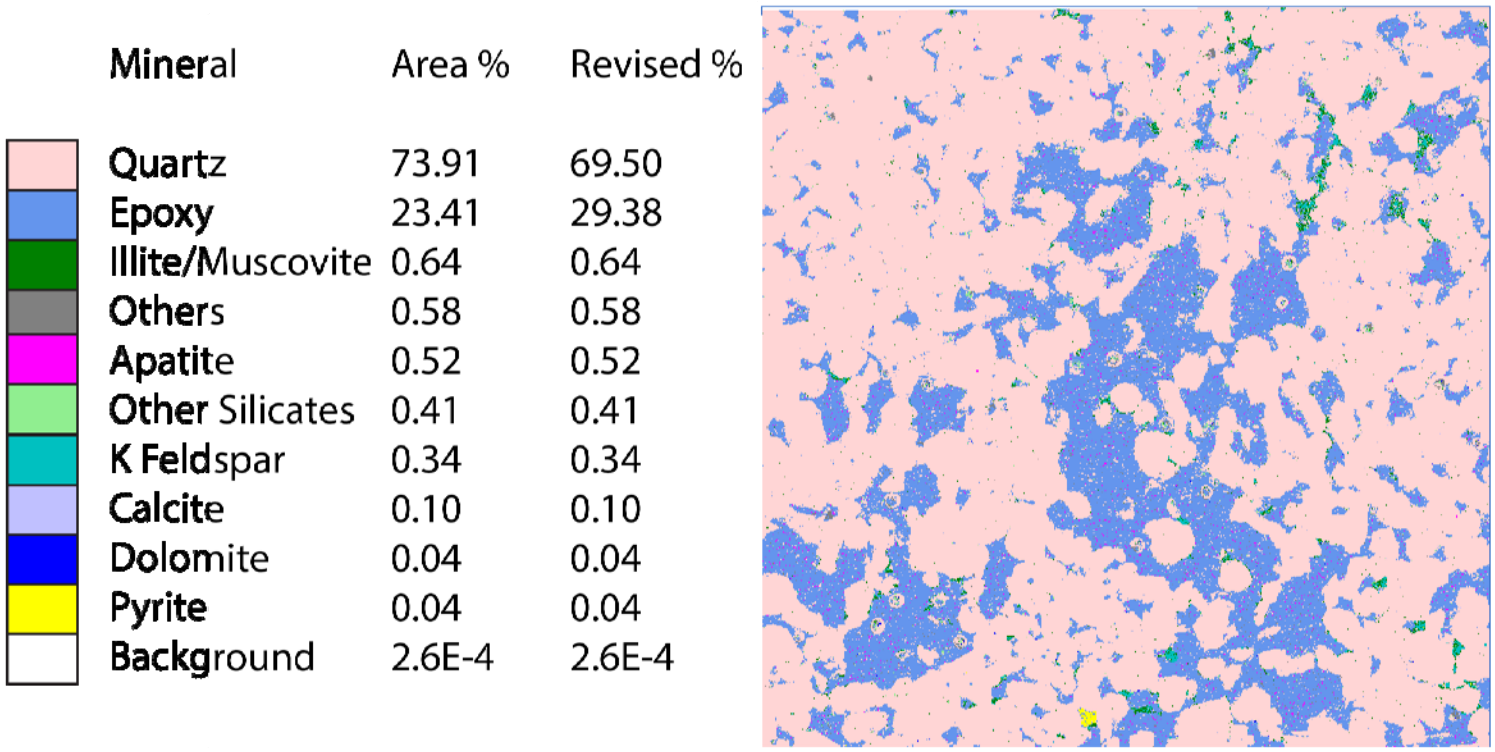

Figure 19: QEMSCAN results for sample #5 (Table 1) showing initial results as well as corrections from manual point count of porosity (epoxy).

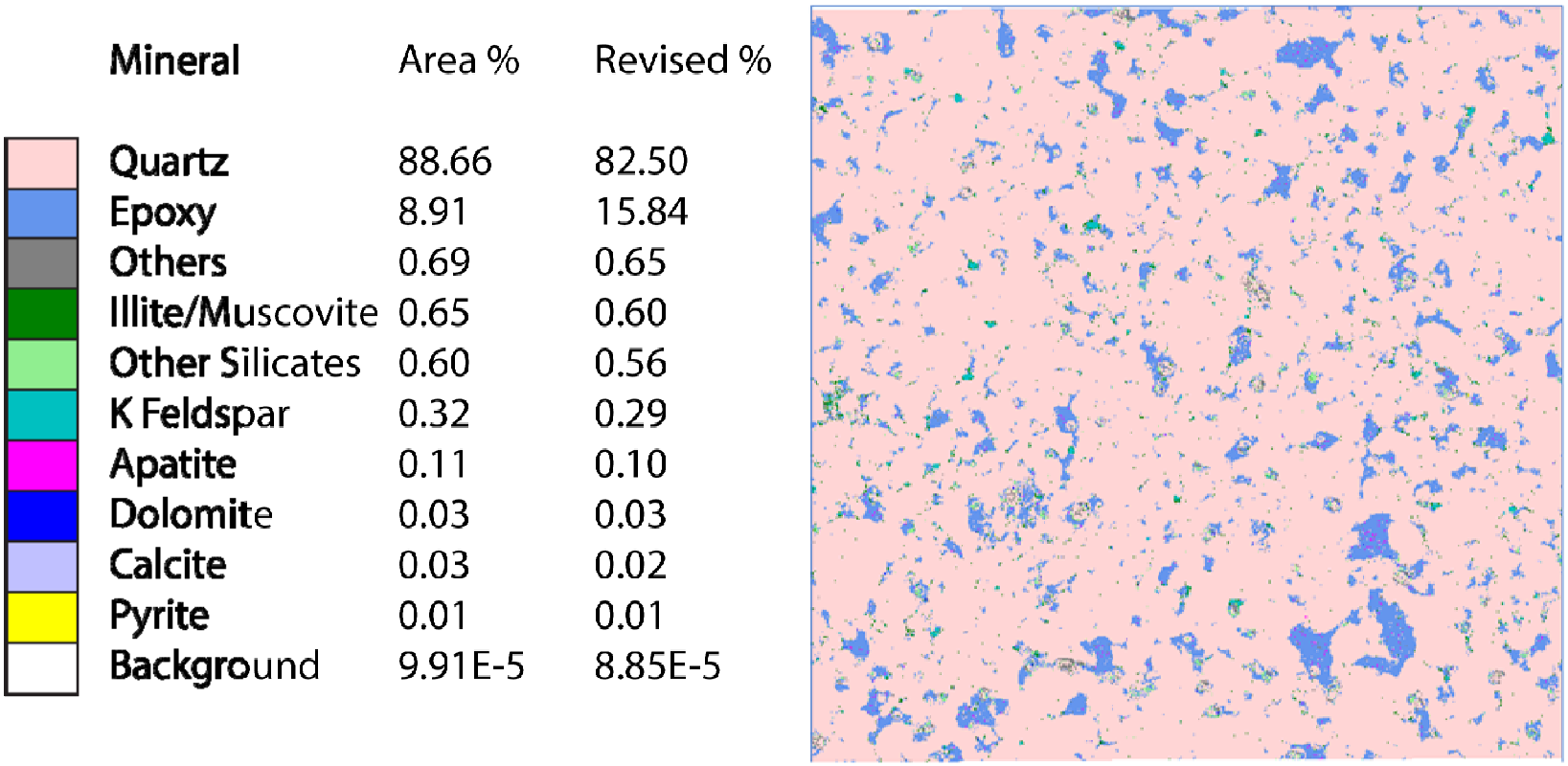

Figure 20: QEMSCAN results for sample #4 (Table 1) showing initial results as well as corrections from manual point count of porosity (epoxy).

Table 1: Depth, porosity and hydraulic conductivity of core samples collected for this study. Coordinates are projected into NAD83 datum.

Sample #	Latitude	Longitude	Stratigraphic Unit	Depth (m)	Porosity	Conductivity (m/yr)
1	38.599222	-95.836365	Marmaton Group	186-187	-	7.03E-3
2	39.571112	-95.589641	Mississippian	660-662	-	1.15E-1
3	41.823844	-94.372357	Maquoketa	427-429	-	7.20E-4
4	41.823844	-94.372357	St. Peter Sandstone	615-617	15%	5.57E2
5	38.874441	-96.310714	St. Peter Sandstone	1015-1017	9%	1.40E1
6	41.823844	-94.372357	Arbuckle Group	561-562	-	1.61E-4

Table 2: Hydraulic parameters used for base case scenario. Anisoptropy and longitudinal dispersivity were constant throughout the grid, with $K_h/K_v = 10$ and dispersivity = 20 m.

Stratigraphic Unit	K_h (m/year)
Upper Pennsylvanian/Permian	30
Missourian Sequence	54.1
Cherokee Group	16.9
Mississippian Limestones	0.27
Hunton Group	50
Maquoketa Shale	0.315
Mid-Late Ordovician	0.063
St. Peter Sandstone	56
Arbuckle Group	65

Table 3: Thermal Properties

Thermal Diffusion Coefficient	0.185 m^2/yr
Thermal Conductivity (solid)	3.59 W/mK
Thermal Conductivity (fluid)	0.85 W/mK
Heat Capacity (solid)	1000 J/kgK
Heat Capacity (fluid)	4186 J/kgK